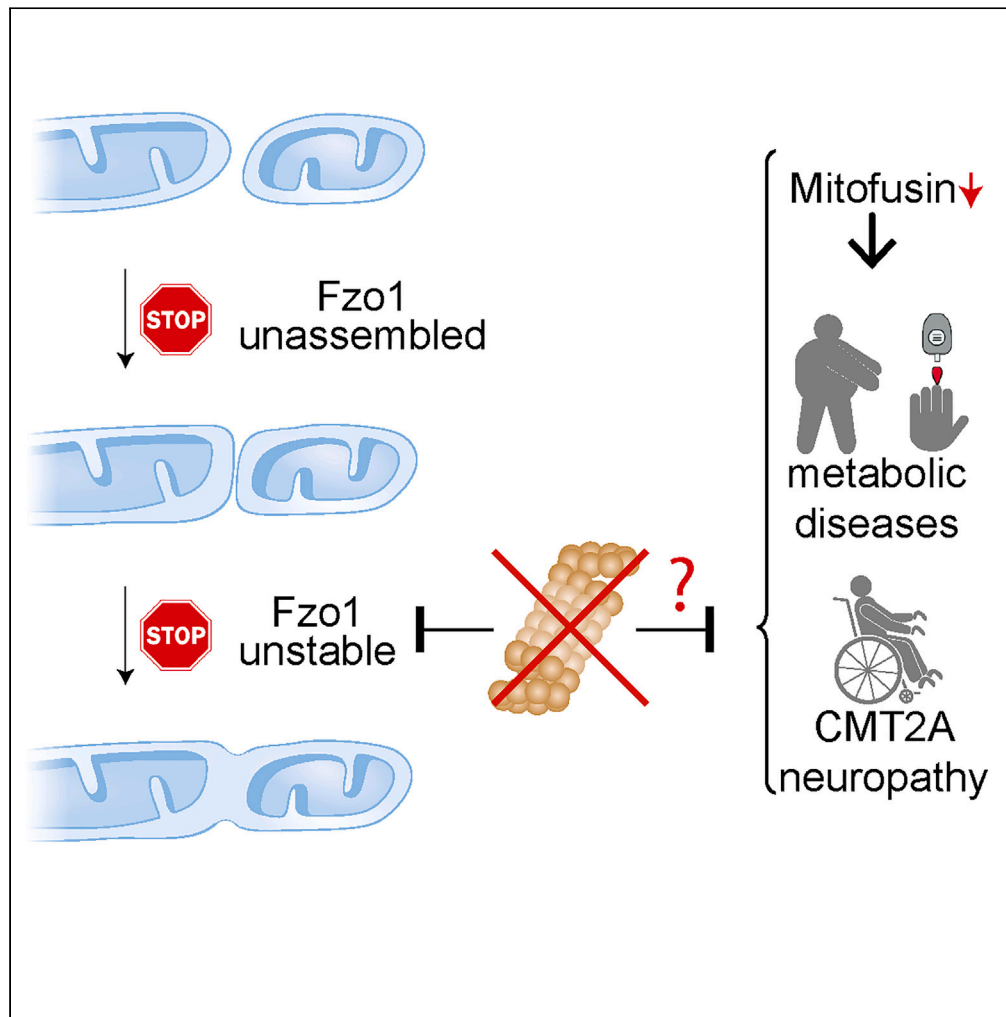


Article

Docking and stability defects in mitofusin highlight the proteasome as a potential therapeutic target



Ira Buntibroich,
Vincent Anton,
Daniel Perez-
Hernandez, ...,
Gunnar Dittmar,
Jan Riemer,
Mafalda Escobar-
Henriques

mafalda.escobar@uni-koeln.
de

Highlights

Two mitofusin cysteines
play hierarchical roles in
mitochondrial fusion

Mitofusin cysteine
mutants reveal two novel
steps in the fusion process

Dysfunctional mitofusins
are rescued by
proteasomal inhibition

Proteasomal inhibition
appears as a promising
therapeutic target

Buntibroich et al., iScience
26, 107014
July 21, 2023 © 2023 The
Author(s).
[https://doi.org/10.1016/
j.isci.2023.107014](https://doi.org/10.1016/j.isci.2023.107014)



Article

Docking and stability defects
in mitofusin highlight the proteasome
as a potential therapeutic target

Ira Buntibroich,¹ Vincent Anton,¹ Daniel Perez-Hernandez,⁵ Tânia Simões,¹ Felix Gaedke,² Astrid Schauss,² Gunnar Dittmar,⁵ Jan Riemer,^{2,4} and Mafalda Escobar-Henriques^{1,2,3,6,*}

SUMMARY

Defects in mitochondrial fusion are at the base of many diseases. Mitofusins power membrane-remodeling events via self-interaction and GTP hydrolysis. However, how exactly mitofusins mediate fusion of the outer membrane is still unclear. Structural studies enable tailored design of mitofusin variants, providing valuable tools to dissect this stepwise process. Here, we found that the two cysteines conserved between yeast and mammals are required for mitochondrial fusion, revealing two novel steps of the fusion cycle. C381 is dominantly required for the formation of the *trans*-tethering complex, before GTP hydrolysis. C805 allows stabilizing the Fzo1 protein and the *trans*-tethering complex, just prior to membrane fusion. Moreover, proteasomal inhibition rescued Fzo1 C805S levels and membrane fusion, suggesting a possible application for clinically approved drugs. Together, our study provides insights into how assembly or stability defects in mitofusins might cause mitofusin-associated diseases and uncovers potential therapeutic intervention by proteasomal inhibition.

INTRODUCTION

Mitochondria are dynamic organelles constantly adapting their shape in response to environmental changes, by balancing fusion and fission processes.^{1,2} This equilibrium is essential for cellular homeostasis.^{3,4} Mitochondrial DNA (mtDNA) maintenance and oxidative phosphorylation depend on mitochondrial fusion.^{5–7} In turn, fragmentation ensures proper mitochondrial distribution and inheritance and allows segregation of damaged mitochondria.⁸ While most membrane fusion events rely on SNARE (soluble N-ethylmaleimide-sensitive-factor attachment receptor) proteins, mitochondrial fusion and fission are mediated by large dynamin-related GTPases (DRPs). Their activity requires self-oligomerization and conformational changes, dependent on GTP hydrolysis.⁹

Mitofusins, Fzo1 in yeast and MFN1/2 in mammals, mediate mitochondrial outer membrane (OM) fusion.¹⁰ They are anchored to the OM via one or two transmembrane (TM) domains, close to the C-terminus.^{11–13} Structural analysis of their bacterial homolog BDLP (bacterial dynamin-like protein) and of truncated versions of MFN1/2, called minimal-GTPase domain (MGD),^{14–17} revealed its arrangement properties. After a globular, N-terminal GTPase domain (G domain), mitofusins fold into two helix bundles (HBs), called HB1 and HB2^{18,19} (Figure 1A).

Mutations in the human mitofusin 2 gene cause the peripheral neurodegenerative disorder Charcot-Marie-Tooth type 2A (CMT2A).^{20,21} Moreover, low levels of mitofusin 1 and 2 are associated with metabolic diseases, like non-alcoholic fatty liver disease (NAFLD),²² and with cardiac and other neurodegenerative diseases.²³ The cascade of events enabling mitofusins to merge two outer mitochondrial membranes is best elucidated for the yeast mitofusin Fzo1.^{24–27} Functional analysis of mitofusin mutant variants allowed dissecting this hierarchical stepwise mechanism.^{15,16,28–30} In this context, cysteines are particularly interesting residues to study, due to their availability, chemical properties, and role in mammalian mitofusins.

Cysteines are very rare amino acids, usually either involved in intermolecular or intramolecular stabilization, by forming disulfide bonds, or involved in the regulation of enzymatic activity, due to their ability to get

¹Institute for Genetics, University of Cologne, Cologne 50931, Germany

²Cologne Excellence Cluster on Cellular Stress Responses in Aging-Associated Diseases (CECAD), University of Cologne, Cologne 50931, Germany

³Center for Molecular Medicine Cologne (CMCC), University of Cologne, Cologne 50931, Germany

⁴Institute for Biochemistry, University of Cologne, Cologne 50931, Germany

⁵Proteomics of Cellular Signaling, Luxembourg Institute of Health, Strassen 1445, Luxembourg

⁶Lead contact

*Correspondence: mafalda.escobar@uni-koeln.de

<https://doi.org/10.1016/j.isci.2023.107014>



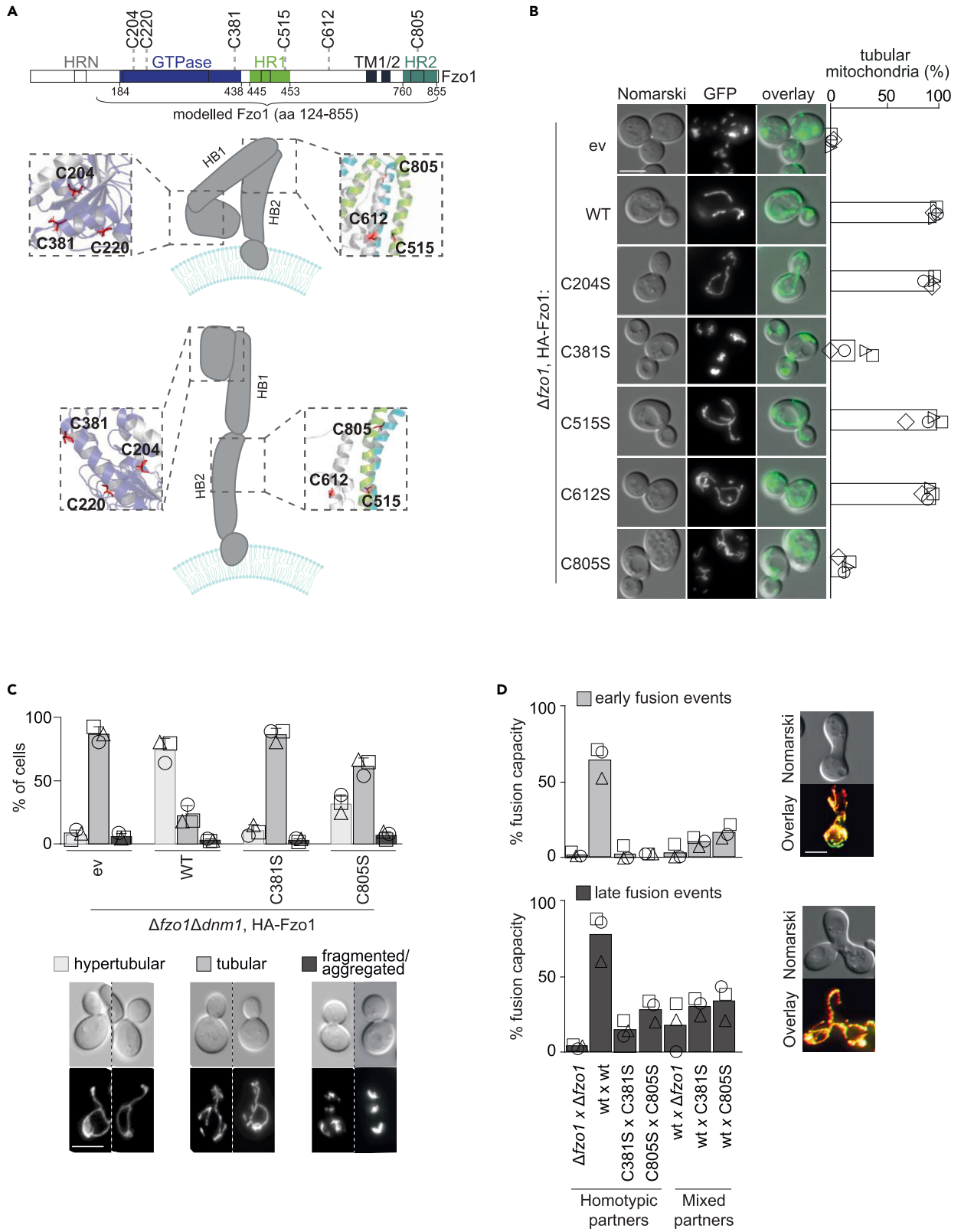


Figure 1. Fzo1 cysteines 381 and 805 are required for mitochondrial fusion

(A) Upper panel: Fzo1 linear structure and localization of the six cysteine residues present in Fzo1. HRN, HR1, HR2: heptad repeat domain; GTPase: GTPase domain; TM1/2: transmembrane domains. Lower panel: Schematic model of Fzo1 based on the bent and stretched conformations of BDLP.^{18,19} Zoom in on C204, 220, and 381 is shown in Fzo1 modeled on MFN1-MGD, either bound to GDP- AlF_4^- (top: PDB: 5GOM)¹⁵ or bound to GDP- BeF_3^- (bottom: PDB: 5YEW).¹⁶ Zoom in of C515, 612, and 805 is shown in Fzo1 modeled on BDLP, either GDP-bound (top; PDB: 2J69; bent conformation)¹⁸ or GMPPNP-bound (PDB: 2W6D; stretched conformation).¹⁹ HB1, HB2: helix bundle(s).

(B) Mitochondrial morphology of cysteine mutant variants. Mitochondrial matrix targeted (mt) tagged GFP (green fluorescent protein) was co-expressed with the indicated cysteine mutant variants of Fzo1, or with the respective empty vector (ev), in cells lacking endogenous *FZO1*, called $\Delta fzo1$. Cellular (Nomarski) and mitochondrial (mtGFP) morphology were visualized by fluorescence microscopy. Mitochondrial morphology was quantified from four individual experiments with more than 200 cells each and is displayed as mean and individual values. Scale bar: 5 μm .

(C) Mitochondrial morphology of cysteine mutant variants in the absence of mitochondrial fission. The indicated HA-tagged variants of Fzo1 were expressed in cells lacking *DNM1* and *FZO1*, analyzed as indicated in (B) and displayed as mean and individual values. Representative images of all mitochondrial morphology states are shown. Scale bar: 5 μm .

(D) *In vivo* mating fusion assay. $\Delta fzo1$ cells (Mata-BY4741 or Mat α -BY4742 strains, respectively) expressing the indicated Fzo1 variants and either mtGFP or mtRFP (red fluorescent protein) were mated. Homotypic and heterotypic mating was performed and fluorophore mixing events are scored, in early mating stages (i.e., early fusion events, present in unbudded zygotes) and in late mating stages (i.e., late fusion events, present in budded zygotes), as illustrated in the representative images, from three independent experiments with at least 50 mated events each, being displayed as mean and individual values. Scale bar: 5 μm .

oxidized. Cysteines in MFN1 and MFN2 were shown to mediate mitochondrial hyperfusion in response to the cellular metabolic status.^{13,31,32} Indeed, the presence of oxidized glutathione (GSSG) induces disulfide bond formation within the mammalian MFNs, leading to stabilization of mitofusin oligomers and enhanced GTP hydrolysis.³² Moreover, disulfide bonds on the MFN2 cysteine 684 mediate these redox-induced alterations of MFN2 oligomerization and stimulate mitochondrial hyperfusion, allowing to adapt mitochondrial shape and respiration to the intra-cellular redox state.³¹ Finally, accessibility studies placed the C-terminus of MFNs and its redox-sensitive cysteine residues in the intermembrane space (IMS) of mitochondria, which implies that reversible redox-mediated disulfide-bond formation occurring in the IMS adapt mitochondrial fusion to the cellular oxidizing state.¹³

Here, we show that the conserved Fzo1 cysteine residue C381 and the partially conserved residue C805 are critical for mitochondrial fusion. C381 is required for G domain interactions *in trans*, while C805 is important for Fzo1 protein stability. Fzo1^{C805S} variants are degraded by the proteasome, preventing fusion, which can be rescued upon proteasomal inhibition. Therefore, the proteasome might be a putative therapeutic target in diseases associated with low levels of MFN1 and MFN2.

RESULTS**Conserved cysteine residues in Fzo1 modulate mitochondrial fusion capacity**

Cysteines are rare and highly reactive residues, thanks to their thiol side chains, thus participating in a myriad of essential enzymatic reactions.^{33–36} Fzo1 possesses six cysteine residues, three of them located in the G domain, the other three in the HB2 (Figures 1A and S1). However, their role in constitutive OM fusion and stabilizing effect during Fzo1 conformational changes is not known. To assess their importance, we exclusively expressed individual cysteine mutant variants in a strain deleted for endogenous *FZO1*, called $\Delta fzo1$, and analyzed mitochondrial morphology, visualized by mitochondrial-targeted GFP. Mitochondrial morphologies were classified as either tubular or non-tubular, which comprises heterogeneous small tubules, dispersed mitochondrial fragments or mitochondrial aggregates. As expected, the reintroduction of wild-type (WT) Fzo1 in $\Delta fzo1$ cells rescued mitochondrial tubulation (Figure 1B). The cysteine residues C381 and C805 were important for mitochondrial reticulation, suggesting impaired Fzo1 functionality (Figure 1B). Interestingly, according to the alignment results, C381 and 805 are the most conserved cysteine residues among mitofusins and may therefore have analogous functions: C381 is totally conserved and 805 is present in the same region as MFN2 C700 (herein referred to as conserved and partially conserved, respectively) (Figures S1 and S2). Both mutant variants were causative for non-tubular mitochondria, however in different ways. Fzo1^{C381S} led to strongly aggregated mitochondria. In contrast, mutation of C805 led to very short and thin mitochondrial tubules, suggesting that residual fusion might still be possible. However, loss of mitochondrial tubulation could also be caused by an increase in mitochondrial fission. Thus, mitochondrial morphology was analyzed in the absence of the fission factor Dnm1 (Figure 1C). As expected, in the absence of both fusion and fission components, mitochondria presented a wt-like tubular morphology (Figure 1C). Moreover, the re-expression of WT Fzo1 induced a hypertubular mitochondrial network, as expected for a $\Delta dnm1$ strain. In contrast, expression of the cysteine variants

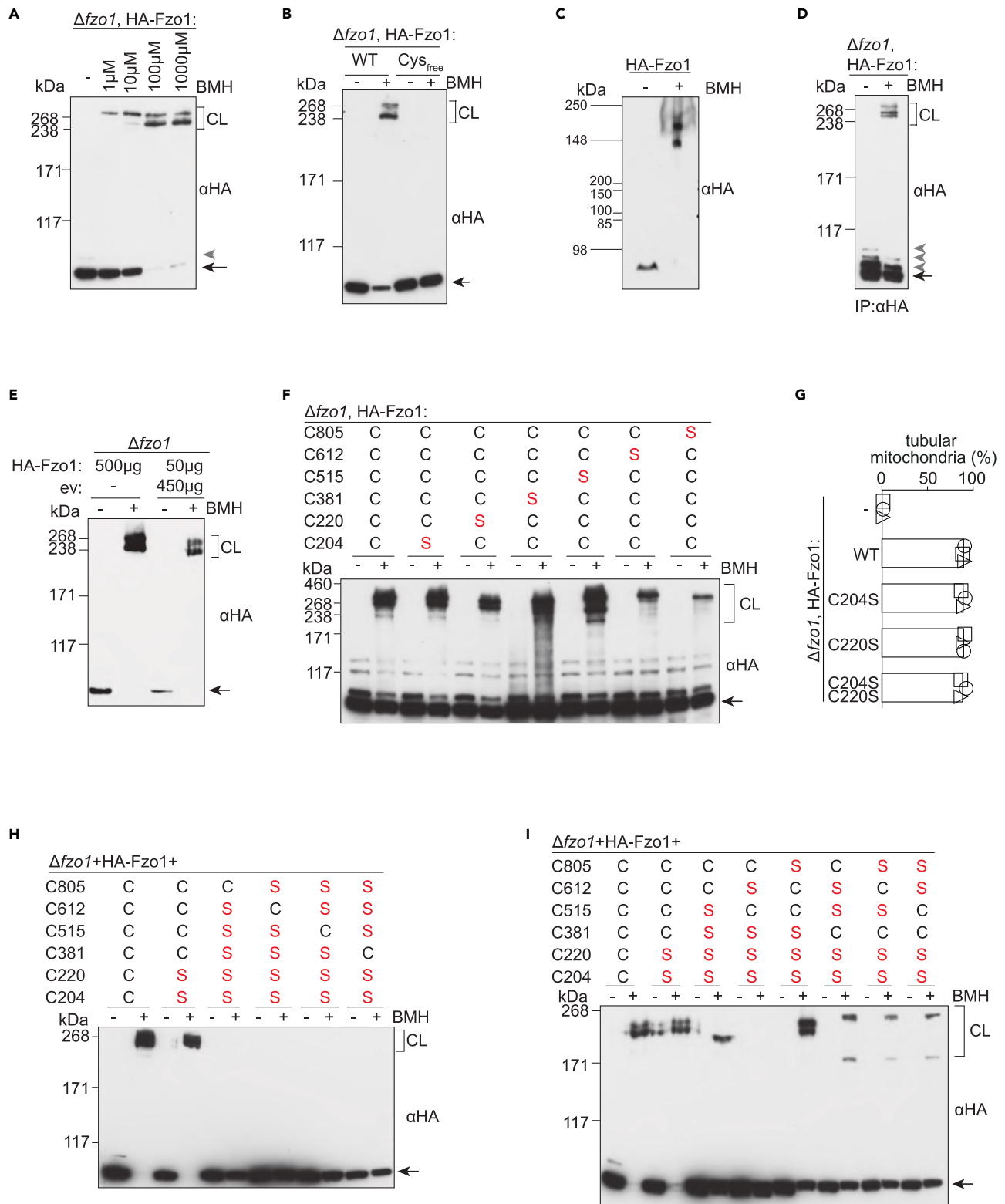


Figure 2. Analysis of Fzo1 cross-linking properties

(A) Crude mitochondrial extracts of $\Delta fzo1$ cells expressing HA-Fzo1, corresponding to 100 μg total protein, were treated with the indicated amounts of cross linker BMH or with DMSO (-) for 30 min, centrifuged, and resuspended in sample buffer containing DTT and analyzed via SDS-PAGE and immunoblotting, using HA-specific antibodies.

Figure 2. Continued

(B) Cross-linking analyses were performed as indicated in (A), but with WT or a 6XCys to Ser variant (Cys_{free}) of HA-Fzo1.

(C) Cross-linking analysis as in (A) but using two different commercially available protein markers.

(D) HA-Fzo1 was purified from solubilized crude mitochondrial extracts using 150 OD₆₀₀ cells, by immunoprecipitation on HA-beads. Precipitated Fzo1 was treated with 100 μ M BMH, before elution with sample buffer containing DTT and subsequently analyzed by immunoblotting, as indicated in (A).

(E) Crude mitochondrial extracts of Δ fzo1 cells expressing HA-Fzo1 or expressing the corresponding empty vector (ev) were mixed as indicated, centrifuged, and cross-linked as in (A).

(F, H, and I) Cross-linking analysis were performed as indicated in (A), with cells expressing the indicated Fzo1 variants.

(G) Mitochondrial morphology was analyzed and scored, as in Figure 1B, and is displayed as mean and individual values. CL: cross linker; BMH: bismaleimido-hexane (13 Å). Unmodified Fzo1 bands are labeled with black arrows. Gray arrowheads show ubiquitylated forms of Fzo1.

Fzo1^{C381S} and Fzo1^{C805S} could not support hypertubulation, confirming a fusion defect, especially present in Fzo1^{C381S}. Finally, to evaluate the fusion capacity of both Fzo1 cysteine variants in a dynamic manner, early and late fusion events were scored by using *in vivo* mating assays.^{28,37} Cells expressing different mitochondrial-targeted fluorophores are mated and colocalization of these fluorophores is monitored. Early fusion events of mitochondria are defined by fluorophore colocalization just after the fusion of the mated cell pair, showing the morphology exemplified in Figure 1D, upper panel. They indicate very rapid and efficient fusion. Late fusion events of mitochondria are defined by fluorophore colocalization in cells where the fused/mated cell pair already progressed toward the formation of the diploid protrusion, as exemplified in Figure 1D, lower panel. This allows more time for fusion to occur and thus reflects less efficient fusion. These analyses confirmed impaired mitochondrial fusion upon expression of Fzo1^{C381S} or Fzo1^{C805S} (Figure 1D, homotypic partners). Moreover, only cells harboring WT Fzo1 on both fusion partners were capable of efficient fusion (Figure 1D, mixed partners), revealing that C381 and C805 must be present on both sides of opposing mitochondria. In conclusion, C381 and C805 are important for mitochondrial fusion.

Fzo1 cysteines regulate fusion independently of disulfide-bond formation

Next, we investigated the role of C381 and C805 in the fusion process. OM fusion occurs through a multistep mechanism, requiring dynamic conformational changes, along with Fzo1 oligomerization, prior to membrane fusion.²⁷ To test whether cysteines must come into proximity during different steps of the fusion cycle, which would be essential for the formation of disulfide bonds, we established an assay to determine complex formation via cross-linking (CL). The cysteine specific cross linker bismaleimido-hexane (BMH), known to link sulfhydryl groups of cysteines, shifted Fzo1 from its monomeric state to Fzo1 oligomers, in a dose-dependent manner (Figure 2A), which were lost in an Fzo1 cysteine-free variant (Figure 2B), as expected. However, the molecular weight of these oligomeric structures could not be reliably estimated, given that the protein standard markers commercially available are not consistent in these higher molecular weight areas (compare Figures 2A and 2C). Therefore, we will call the CL species "oligomers", as they are clearly distinguishable from the unmodified Fzo1 monomer. BMH induced similar shifts to Fzo1 previously purified by immunoprecipitation (Figure 2D), suggesting that these oligomers might be due to Fzo1 self-interaction. During the fusion cycle, Fzo1 oligomerizes in *cis* and evolves to higher oligomeric structures upon *trans* apposition between two mitochondria.³⁸ Therefore, we investigated if the oligomeric status of cross-linked Fzo1 is affected by mitochondrial tethering. *In vitro*, this can be mimicked by 10x concentration and centrifugation of isolated mitochondria, which favors their contact in *trans*. This is compared to 10x concentrated mitochondria but where only 1/10 of mitochondria contain Fzo1, and the other 9/10 comprise mitochondria from Δ fzo1 cells, to prevent potential *trans* interactions. The Fzo1 cross-linked oligomer was similar under concentrated or ten times diluted Fzo1-mitochondria, suggesting that BMH only cross-links Fzo1 oligomers in *cis* (Figure 2E). Importantly, single cysteine mutations in Fzo1 were not sufficient to completely prevent oligomer formation (Figure 2F). We then aimed at analyzing if one single cysteine in Fzo1 would be sufficient to form the cross-linked oligomeric complex. For simplicity, we first created the double mutant Fzo1^{C204S, C220S}, which was still able to mediate fusion (Figure 2G) and form WT-like oligomeric structures (Figure 2H). Therefore, we excluded a function of the residues C204 and C220 for oligomer formation. Further mutations, constructed to allow testing single cysteines individually, showed that cross-linking required more than one cysteine in Fzo1 (Figure 2H), suggesting Fzo1 cysteines do not form homotypic disulfide bonds. To analyze which residues allowed Fzo1 cross-linking, we created mutant variants encoding all possible cysteine pairs. We noticed that the cysteine pair 612 and 515 were required for the WT-like oligomer formation (Figure 2I). In contrast, even though the presence of C381 in combination with a second cysteine allowed the formation of Fzo1 cross-linked species, they appeared very different from the WT oligomer and were not further investigated. Together, these results indicate that C381 and C805 regulate Fzo1 and mitochondria fusion independently of homotypic or heterotypic disulfide bond formation.

Trans-association of Fzo1 requires cysteines 381 and 805

We further analyzed the importance of C381 and C805 for Fzo1 conformations, profiting from the fact that their mutant variants still allow the formation of the CL oligomer. After CL addition, we performed tryptic digestion, followed by mass spectrometric analysis, and compared the peptide profile of Fzo1 WT, C381S, and C805S. We expect that conformational alterations will reveal differences in the open regions, accessible to digestion and thus generating more peptides. When compared to WT Fzo1, the profile of the C381S mutant shows many more peptides, appearing especially in the middle of the protein (Figure S3). In contrast, the C805S variant presented a tryptic profile similar to WT Fzo1. These results substantiate a different effect of C381 and C805 in Fzo1 conformations: while C805S does not appear to cause major alterations in Fzo1 CL oligomers, C381S seems to induce big differences in the conformation of Fzo1.

Next, we investigated the role of C381 and C805 in Fzo1 oligomeric complexes in *trans*, i.e., upon mitochondrial tethering. *Trans* association of Fzo1 can be fostered by centrifugation of isolated mitochondria, followed by sucrose gradient analysis.³⁸ As expected, WT Fzo1 peaked at the density corresponding to the *trans*-oligomer (Figure 3A). In contrast, the Fzo1^{C381S} mutant peaked at the density corresponding to the *cis*-oligomer, showing that cysteine 381 is essential for the *trans* oligomerization of Fzo1. In fact, modeling of Fzo1 to the available crystal structures predicts the cysteine 381 to locate at the surface of the G domain, which was shown to act as a dimerization interface, required for *trans*-assembly of mitofusins (Figure 1A).^{15,16,39} In contrast, the mutant variant Fzo1^{C805S} partially but consistently shifted the complex to a lower fraction, suggesting the formation of *trans* complexes which are unstable (Figure 3B). In fact, C805 is located in helix bundle 2, which could be important to stabilize the *trans*-oligomerization of Fzo1 (Figures 1A and S2B).³⁰ In conclusion, the cysteine residues 381 and 805 are both required for *trans*-oligomerization of Fzo1, albeit differently.

Cysteines 381 and 805 in Fzo1 regulate successive steps in the fusion process

After *trans* assembly, GTP is hydrolyzed, inducing conformational changes that allow ubiquitylation of Fzo1, an essential step in mitochondrial fusion.^{28–30,38,40,41} To further understand the differential roles of the residues C381 and C805, we analyzed the protein level and ubiquitylation of the Fzo1 mutants thereof. While C381 Fzo1 mutants showed increased steady-state protein levels, along with impaired ubiquitylation, C805 Fzo1 mutants presented a very low abundance, but only showed a mild decrease of ubiquitylation (Figures 3C, S4A, and S4B). Both cysteine and histidine residues can perform metal coordination, in which case their exchange is expected to maintain functionality. However, replacement of either cysteine 381 or 805 by histidine did not rescue Fzo1 levels or ubiquitylation, rendering their role in metal ion binding highly unlikely. Moreover, mutation of C381 to serine, alanine, or histidine had the same detrimental effect on mitochondrial tubulation (Figure S4C), revealing the essential role of this residue for Fzo1 functionality. Interestingly, the mutant Fzo1^{C381H} affected Fzo1 levels and ubiquitylation even more severely than Fzo1^{C381S} (Figure S4A). Fzo1 C381 is located in helix α 4 of the G domain, directly in the GTPase dimerization interface (Figure S4D). This region undergoes structural rearrangements that are required for oligomerization, GTPase activity, ubiquitylation, and fusogenic capacity.²⁹ Therefore, the bulkiness of histidine, compared to alanine and serine, might strongly affect this conformation dynamism.

To further explore the role of C381 and C805, we analyzed the protein stability of the variants Fzo1^{C381H} and Fzo1^{C805S}, using cycloheximide (CHX) chase analysis (Figure 3D). Consistent with the absence of Fzo1 ubiquitylation and higher steady-state levels, the mutation C381H stabilized Fzo1. In contrast, the mutation C805S destabilized Fzo1, as expected from its decreased steady-state levels. Interestingly, mutation of MFN2 C700, the counterpart residue of yeast C805, leads to reduced protein state levels, in line with our results in yeast.³² Based on our analyses so far, C381 plays an important role in the early steps of the fusion cycle whereas C805 only becomes important at a late stage. This would suggest that the combination of both cysteine mutations should show the same phenotypes as C381H alone, as the cycle is blocked in an early step already. Consistently, a dominant effect of C381H over C805S was revealed in ubiquitylation (Figure 3C), protein stability (Figure 3D), and *trans*-complex formation of Fzo1 (Figure 3E). In sum, the most conserved cysteines 381 and 805 are required at different steps during OM fusion and mutations in the residue 381 are dominant over mutations in 805.

Impairment of C381 prevents mitochondrial docking

During OM fusion, mitochondria transit from a tethered to a docked state, characterized by a tight apposition and flattened shape of the apposed membranes⁴¹ (Figure 4A). We previously found that K464

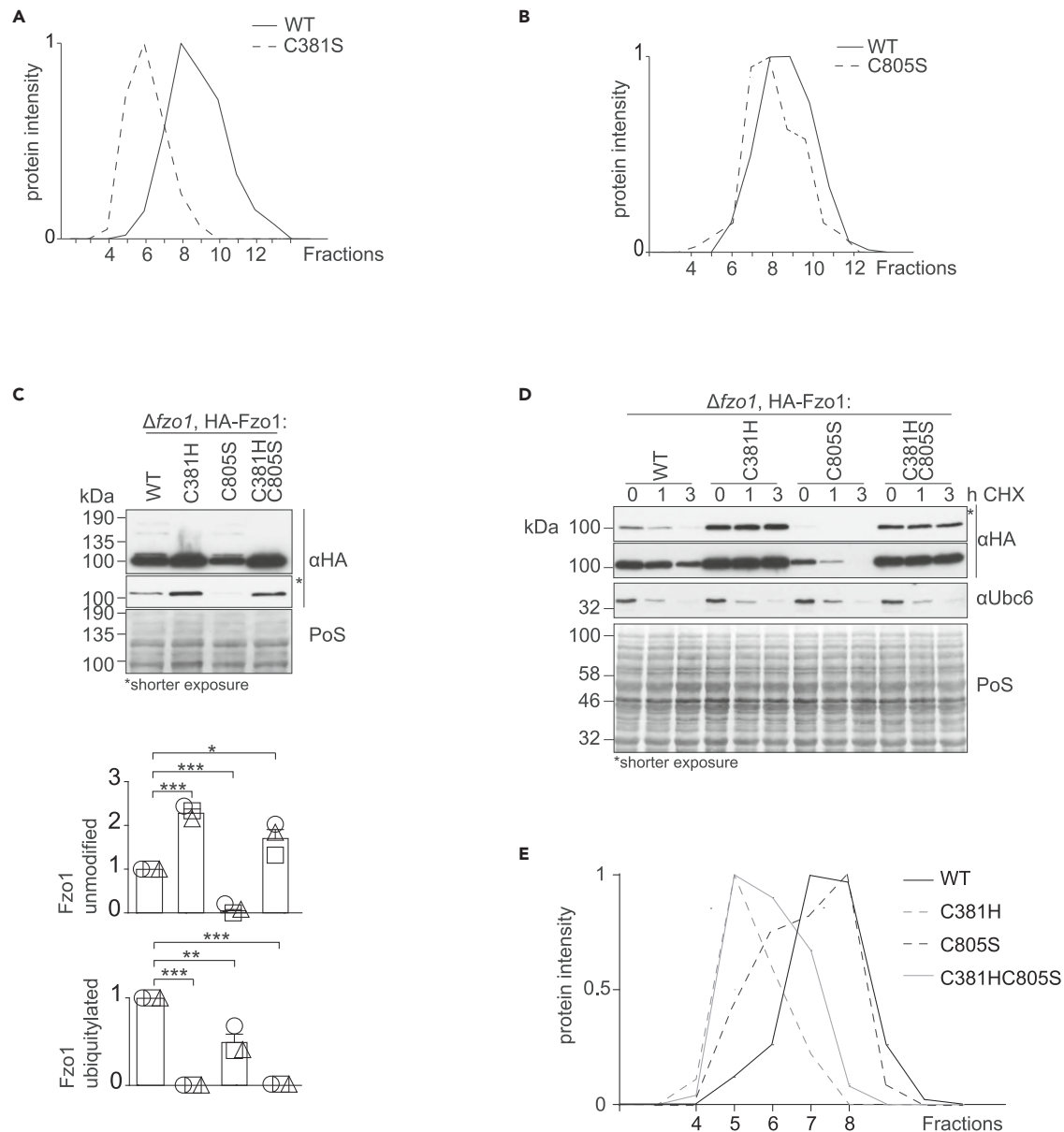


Figure 3. C381-loss phenotypes are dominant over C805

(A and B) Fzo1 complex formation. Sucrose gradient centrifugation was performed with solubilized crude mitochondrial extracts of strains expressing the indicated variants of HA-tagged Fzo1. The gradients were fractionated, proteins were precipitated with trichloroacetic acid, and the samples were analyzed by SDS-PAGE and Western blot, using an HA-specific antibody to quantify the Fzo1 signal.

(C) Fzo1 protein levels. Total cellular protein extracts from $\Delta fzo1$ cells expressing the indicated variants of HA-Fzo1 were analyzed by SDS-PAGE and immunoblotting, using HA-specific antibodies. The Ponceau S (PoS) staining was used as a loading control. Quantification from three individual experiments is displayed as mean and individual values. Significance is indicated as p values displayed as * with $p < 0.05$, ** with $p < 0.01$, *** with $p < 0.001$ and **** with $p < 0.0001$.

(D) Protein stability of Fzo1. $\Delta fzo1$ cells expressing the indicated variants of HA-Fzo1 were treated with the translation inhibitor cycloheximide (CHX). Samples were taken 0, 1, or 3 h after protein synthesis shut off and total protein extracts were analyzed by immunoblotting, as in (C), but additionally using a Ubc6-specific antibody, as an unstable protein control.

(E) Fzo1 oligomerization properties of the indicated Fzo1 variants, as indicated in (A).

mutations still allowed mitochondria to reach the docked state.²⁸ Similarly to C381H, K464 mutations block Fzo1 ubiquitylation. Thus, to better understand the role of C381, we investigated whether Fzo1^{C381H} could reach the docked stage of the fusion process.²⁸ To this aim, mitochondria were isolated from cells

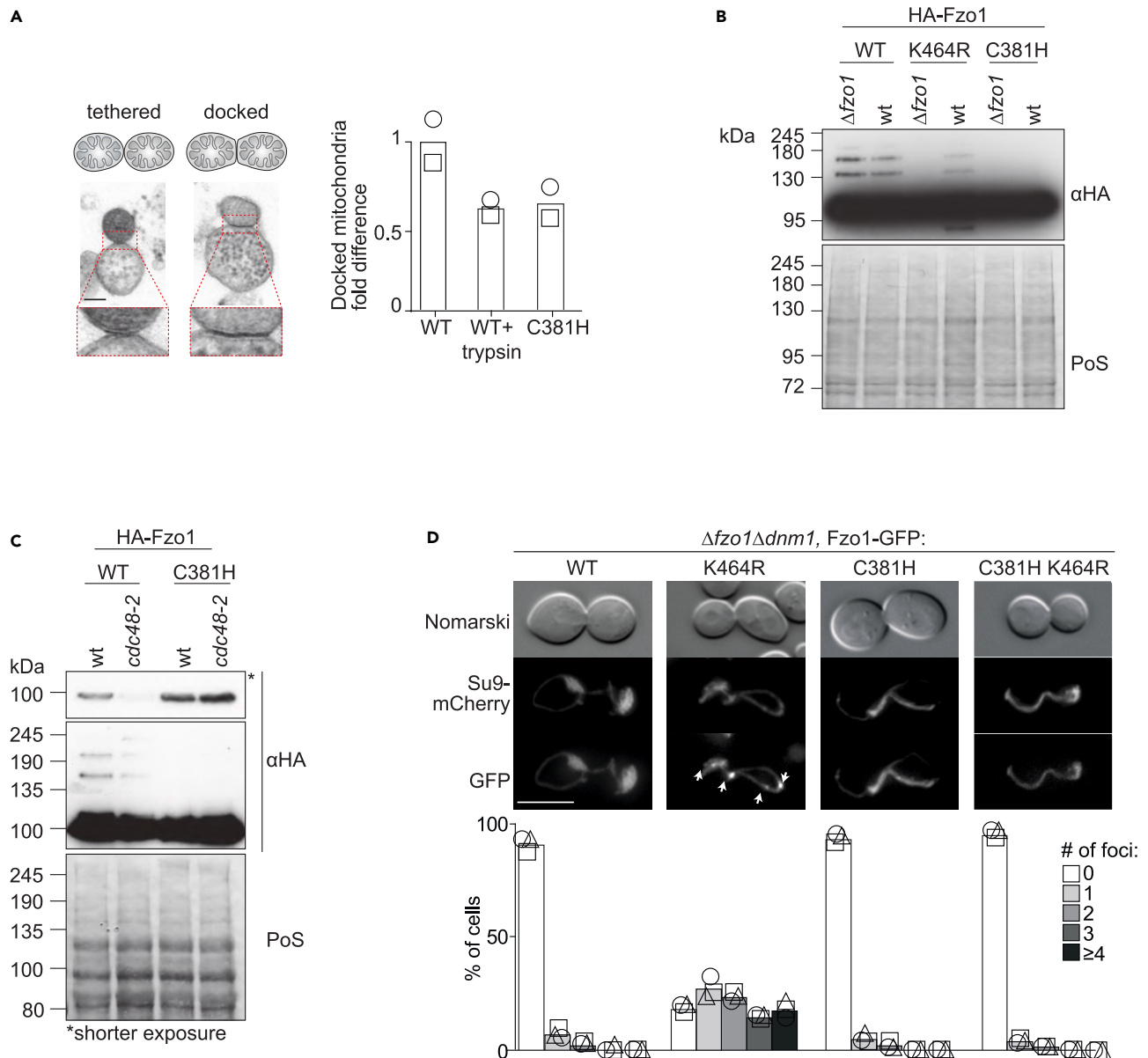


Figure 4. Fzo1 C381 is required for mitochondrial docking

(A) Mitochondrial docking analysis. Mitochondria were purified from *ugo1-2Δfzo1* cells^{28,43} expressing HA-Fzo1 or HA-Fzo1^{C381H} and analyzed by TEM (Transmission Electron Microscopy) for docked events. Isolated mitochondria were treated with 0.5 μg/mL trypsin when indicated. Two independent experiments were quantified as previously described,²⁸ with at least 684 mitochondria each, being displayed as mean and individual values. Shown are representative images of tethered and docked mitochondria (left) and relative docking of mitochondria (right). Scale bar: 100 nm.

(B and C) Fzo1 protein levels. Total cellular extracts of wt and $\Delta fzo1$ cells (B), or of wt and *cdc48-2* cells (C), expressing the indicated HA-tagged variants of Fzo1 were analyzed via SDS-PAGE and immunoblotting using HA-specific antibodies, as described in Figure 3C.

(D) Fzo1 foci formation. Fzo1-GFP foci were analyzed in $\Delta fzo1\Delta dnm1$ cells co-expressing the indicated mutant versions of Fzo1-GFP and the mitochondrial tagged Su9-mCherry. Cellular (Nomarski), mitochondrial (mCherry) morphology and Fzo1 localization (GFP) were visualized by fluorescence microscopy. Fzo1 foci from three independent experiments, with at least 100 cells showing a tubular mitochondrial network each, were counted from three independent experiments, being displayed as mean and individual values. Scale bar: 5 μm.

expressing either WT Fzo1 or Fzo1^{C381H} and membrane deformations were analyzed by electron microscopy (Figures 4A and S5). Moreover, WT mitochondria were treated with the protease trypsin, which degrades Fzo1 and thus prevents docking (Figure 4A, compare WT with WT + trypsin). The C381H mutant resembled the docking deficiency control, suggesting a role of Fzo1 C381 in mitochondrial docking.

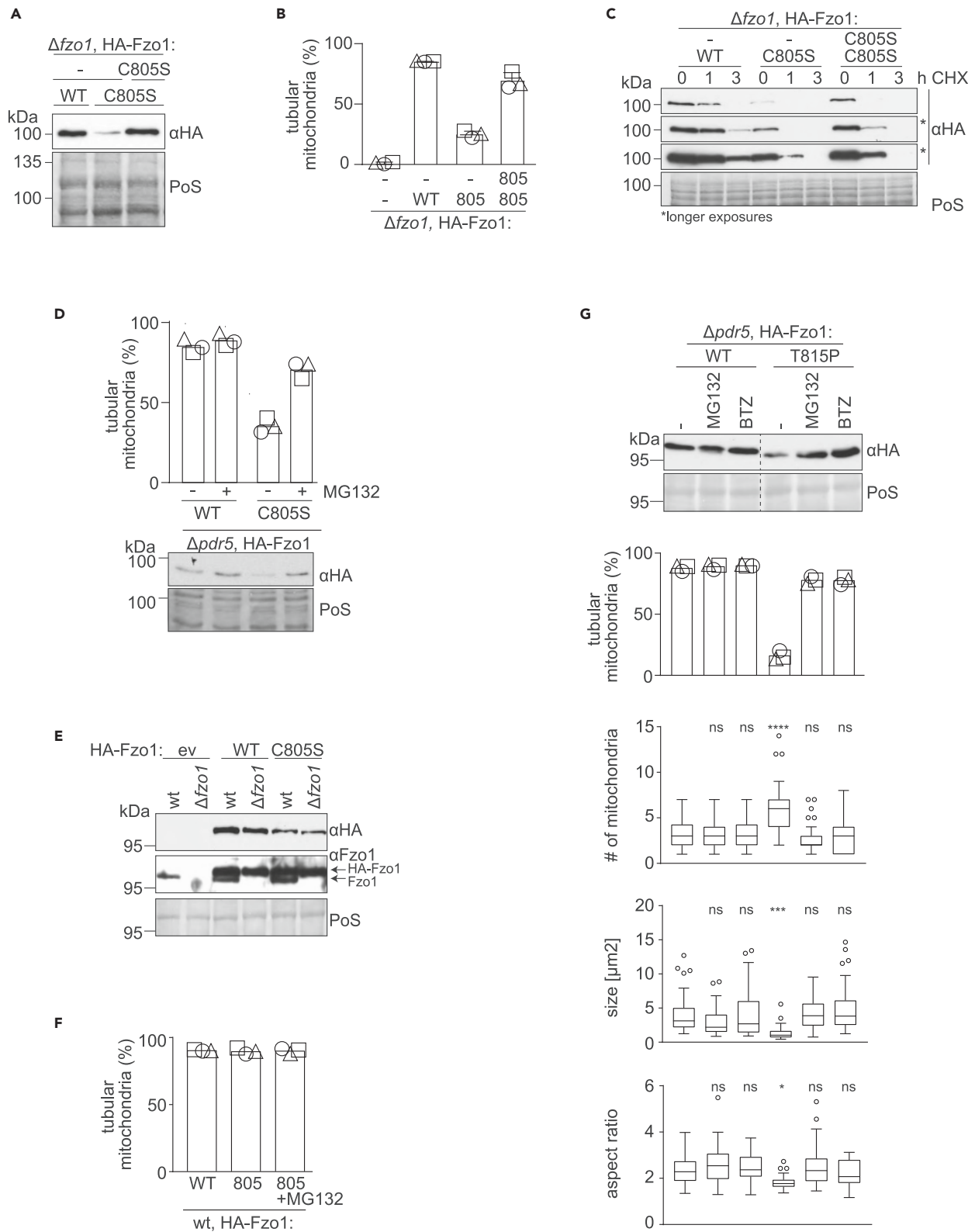


Figure 5. Fzo1 C805 is required for protein stability

(A) Rescue of HA-Fzo1^{C805S} steady state levels by ectopic expression. Total cellular extracts of $\Delta fzo1$ cells co-expressing two plasmids with the indicated HA-Fzo1 variants were analyzed as described in Figure 3C.

Figure 5. Continued

- (B) Increased HA-Fzo1^{C805S} protein levels rescue mitochondrial tubulation. Mitochondrial morphology was analyzed as in Figure 1B using cells as described in (A), displayed as mean and individual values.
- (C) Fzo1^{C805S} degradation properties. CHX chase assays were performed as in Figure 3D using cells as described in (A).
- (D) Proteasomal inhibition rescues fusion (upper panel) and protein levels (lower panel) of HA-Fzo1^{C805S} cells. Mitochondrial morphology was analyzed and quantified as in Figure 1B, being displayed as mean and individual values, but using $\Delta pdr5$ cells expressing genomically integrated HA-Fzo1 or HA-Fzo1^{C805S} and treated with MG132 for 1 h when indicated. For proteasome dependence of Fzo1^{C805S} protein levels, total cellular extracts of the same cells were analyzed, as described in Figure 3C.
- (E) Endogenous Fzo1 levels are unaffected by expression of mutant Fzo1. wt or $\Delta fzo1$ cells expressing an empty vector (ev), HA-Fzo1 or HA-Fzo1^{C805S} were analyzed as in Figure 3C.
- (F) Mitochondrial morphology is unaffected by stabilization of mutant Fzo1. $\Delta pdr5$ cells expressing HA-Fzo1 or HA-Fzo1^{C805S} were treated with MG132 and analyzed as in B.
- (G) The CMT2A disease mutant T815P is stabilized upon proteasomal inhibition. $\Delta pdr5$ cells expressing HA-Fzo1 or HA-Fzo1^{T815P} were analyzed as in D, but using the indicated proteasomal inhibitors. Mitochondrial morphology was quantified as in 1B and additionally evaluated by automated particle analyses using Fiji/ImageJ.⁴⁵ The number of mitochondria, the average size of mitochondria and the mitochondrial aspect ratio, i.e. the ratio of the major to the minor axis, per cell, is represented. Values are displayed as Tukey boxplots. Significance is indicated as p values displayed as * with $p < 0.05$, ** with $p < 0.01$, *** with $p < 0.001$ and **** with $p < 0.0001$, or ns for non significant.

This is in contrast with previous observations with the Fzo1^{K464R} variant, which still allowed mitochondria to reach the docked state, despite blocking Fzo1 ubiquitylation similarly to Fzo1^{C381H}. Thus, C381 is required earlier in the fusion process than K464. To further compare Fzo1^{C381H} and Fzo1^{K464R}, we analyzed in more detail the properties of Fzo1 ubiquitylation, a late step in the fusion process. In fact, we previously noticed that the non-ubiquitylated mutant of Fzo1 K464R can recover ubiquitylation if WT Fzo1 is co-expressed in parallel to the mutant version (Figure 4B, compare lanes 3 and 4).⁴² However, we noticed that the WT protein is unable to rescue ubiquitylation of the C381H mutant protein, as it does for the K464R variant (Figure 4B, compare lanes 5 and 6). This further supports a role of C381, upstream of K464 and GTP hydrolysis. In conclusion, C381 mutations arrest mitochondrial fusion prior to mitochondrial docking.

Impairment of cysteine 381 renders Fzo1 insensitive to Cdc48

Mitochondrial fusion requires the AAA-chaperone Cdc48, which is known to bind ubiquitylated substrates.²⁷ Compromised activity of Cdc48 destabilizes ubiquitylated Fzo1, leading to lower steady-state levels in the hypomorphic *cdc48-2* strain, expressing the variant Cdc48^{A547T44} (Figure 4C). In contrast, consistent with the lack of ubiquitylation, Fzo1^{C381H} is insensitive to the *cdc48-2* mutation. Importantly, after Fzo1 ubiquitylation, Cdc48 disassembles Fzo1 complexes, alleviating steric hindrance and allowing membrane fusion.²⁸ Consequently, upon impairment of Cdc48, or upon K464R mutation, the oligomeric complexes of Fzo1 accumulate in foci on the mitochondria. Thus, we analyzed the role of Fzo1^{C381H} in foci formation. To monitor the distribution of Fzo1 along the mitochondrial network, we assessed co-localization of mCherry targeted to mitochondria with Fzo1-GFP, or with the respective K464 and C381 mutants thereof. Moreover, *DNM1* was deleted, to force mitochondrial tubulation even in the presence of inactive Fzo1 variants. As expected, Fzo1 foci were barely visible in control cells, due to Cdc48 activity, whereas Fzo1^{K464R}-GFP was arrested in puncta (Figure 4D). In contrast, Fzo1^{C381H} did not form foci, consistent with its importance before mitochondrial docking. Finally, a similar behavior could be observed for the double mutant Fzo1^{C381H K464R}, confirming a role for C381 upstream of K464. In sum, the Fzo1^{C381H} mutant variant allowed to identify an additional stage in the fusion process, upstream of mitochondrial tethering and of Cdc48.

Fusion defects of Fzo1^{C805S} are caused by insufficient protein levels

The decreased stability of Fzo1^{C805S} (Figure 3D) prompted us to investigate whether the fusion defects of Fzo1^{C805S} are caused by insufficient protein levels. Co-expression of Fzo1^{C805S} from two low-copy plasmids could restore the protein WT levels (Figure 5A). Importantly, restoring Fzo1^{C805S} expression also rescued fusion capacity (Figure 5B), despite no observable rescue of the turnover rate during CHX treatment (Figure 5C). Fzo1^{C805S} was less affected than WT Fzo1 to the hypomorphic *cdc48-2* mutant (Figure S6A) and less Cdc48 could be co-immunoprecipitated with the mutant C805S when compared to WT Fzo1 (Figure S6B). This is consistent with the previously mentioned roles of Cdc48 in Fzo1 oligomer disassembly²⁸ and C805 in Fzo1 oligomer stability. Importantly, these phenotypes were also caused by the decreased protein levels of Fzo1. Indeed, consistent with a rescue of the fusogenic activity, re-expression of Fzo1^{C805S} to WT-like levels restored WT-like sensitivity of Fzo1 to the mutant variant Cdc48^{A547T} (Figure S6A). Moreover, the decreased binding affinity between Fzo1^{C805S} and Cdc48 was also rescued by re-expression to WT levels of Fzo1^{C805S} (Figure S6B). In conclusion, mutating C805 in Fzo1 does not intrinsically impair its fusogenic capacity.

To further assess the importance of the Fzo1 protein levels, we first investigated if the instability of Fzo1^{C805S} was dependent on the proteasome. Indeed, inhibition of the proteolytic capacity of the proteasome by MG132 treatment rescued Fzo1 protein levels and mitochondrial fusion (Figure 5D, lower and upper panels, respectively). To exclude that stabilizing this non-functional mutant might have a detrimental effect on WT Fzo1, we tested whether expression of Fzo1^{C805S} leads to degradation of endogenous Fzo1. However, endogenous Fzo1 was unaffected by the expression of WT or C805S Fzo1 (Figure 5E). Similarly, expression of Fzo1^{C805S} in the absence or presence of the proteasomal inhibitor MG132 did not impair mitochondrial tubulation in cells expressing endogenous Fzo1 (Figure 5F). This allows us to exclude a dominant detrimental effect for mitochondrial fusion of Fzo1^{C805S}.

To test the proteasomal importance in a disease context, we analyzed the nearby Fzo1 residue T815. According to the alignment results (Figure S1), T815 corresponds to T706 in MFN2, whose mutation to proline is causative of CMT2A neuropathy (Figure S1).⁴⁶ Therefore, despite the divergent sequences between yeast and metazoan in this area, the threonine residues 815 in Fzo1 and 706 in MFN2 are likely present in the same regions and may fulfill similar functions. Importantly, MFN2^{T706}/Fzo1^{T815} is also located close to the C-terminus, known as a potential domain to stabilize Fzo1 oligomers, as previously mentioned.^{25,30,38,47} Thus, we predicted it to behave similarly to Fzo1^{C805S}. Indeed, Fzo1^{T815P} leads to Fzo1 destabilization and mitochondrial fragmentation, phenotypes once again rescued by proteasomal inhibition with MG132 or Bortezomib (BTZ) (Figure 5G). This effect was confirmed by automated quantification of mitochondrial morphology, showing rescue of the number of mitochondria per cell, average mitochondrial size, and aspect ratio (Figure 5G). This demonstrates that in the case of catalytically active Fzo1, conditions leading to protein levels below the threshold required for mitochondrial fusion, e.g. in Fzo1^{C805S} or Fzo1^{T815P}, can be rescued by proteasomal inhibition. In sum, Fzo1^{C805S} mutant variants revealed a quality control step in the fusion cascade, defined by the proper assembly of Fzo1 fusogenic oligomers.

DISCUSSION

Cysteines are rare and highly reactive residues, with a multitude of regulatory roles. For example, cysteines stabilize native protein conformations and mediate conformational changes.^{33–35} Nevertheless, very little is known about how cysteine residues generally regulate the conformational changes inherent to the membrane remodeling properties of the large dynamin GTPase proteins. Here, we investigated the importance of cysteine residues in mitochondrial fusion. We found that mutations in the most conserved cysteines C381 and C805 of the yeast mitofusin Fzo1 arrested the fusion cycle. Our results unravel critical steps in mitochondrial OM fusion.

The multistep process of OM fusion

Mitofusins are membrane-embedded large GTPases and, as such, their functionality relies on several processes. These include membrane insertion, oligomerization, GTP hydrolysis, and interaction with other fusogenic components. Failure in any of these steps probably explains the multitude of diseases linked to mitofusin deficiencies. It also underlines the importance of keeping this complexity in check. Indeed, mitofusins are prominent quality control targets, relevant in cellular homeostasis and affecting mitophagy and cell death, for example.⁴⁸ Not surprisingly, several ubiquitin ligases have been identified to modify mitofusins under many different physiological and stress conditions.⁴⁹

The yeast *Saccharomyces cerevisiae* allowed fundamental basic discoveries and is currently the model organism where OM fusion is best understood.²⁷ After insertion into the OM and GTP binding, the yeast mitofusin Fzo1 oligomerizes in *cis*.³⁸ Then, upon mitochondrial apposition, G-domain interactions allow the formation of higher oligomeric states in *trans* and thus mitochondrial tethering.³⁸ Subsequent conformational changes, powered by multiple rounds of GTP binding and hydrolysis, allow mitochondrial docking and lipid merging.^{28,30,41} Finally, disassembly of the oligomeric complex allows recycling of the fusogenic machinery. This is enabled by ubiquitylation of Fzo1 at a late OM fusion step and subsequent protein complex dissociation by the AAA-protein Cdc48.^{28,29,44}

Identification of critical steps in mitochondrial OM fusion

Our systematic analysis of the importance of cysteine residues for mitochondrial fusion revealed two cysteine residues within the mitofusin Fzo1 as being important for OM fusion, namely C381 and C805.

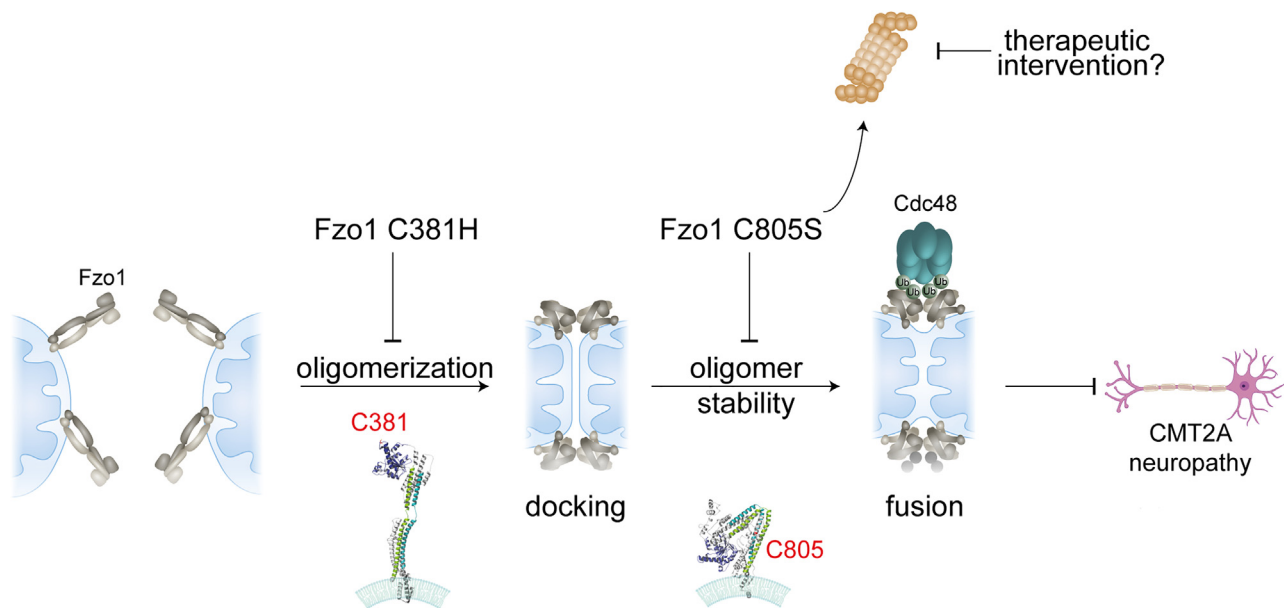


Figure 6. Role of conserved cysteines in mitochondrial outer membrane fusion

Mitochondrial fusion requires outer membrane approximation and tethering, mediated by higher oligomerization in *trans* of the Fzo1 *cis* oligomers from each mitochondrion. GTP hydrolysis then induces conformational changes that allow extensive membrane mitochondrial apposition, defining the docking state, which requires the conserved cysteine C381 in Fzo1, located in the G-G interface. After membrane merging and Fzo1 ubiquitylation, Cdc48 dissociates the Fzo1 complex, recycling it for the next fusion round. The mutation C805S in helix bundle (HB2) destabilizes Fzo1 *trans* oligomers, leading to proteasomal degradation of these complexes and thereby preventing membrane merging. The integrity of this process is essential to ensure mitochondrial plasticity and thereby neuronal health, being its failure causative of CMT2A neuropathy. The direct regulation of faulty Fzo1 complexes by the proteasome renders proteasomal inhibition as an attractive putative target for therapeutic interventions. The neuron image was created with [Biorender.com](https://www.biorender.com).

C381 and C805 mutations affect Fzo1 protein ubiquitylation and stability, and Fzo1 complex formation, but in opposing ways.

Fzo1-C381 is important for higher complex formation, which occurs upon *trans* contacts between two mitochondria and mediates mitochondrial tethering.²⁸ Consistently, in the Fzo1-C381S mutant, mitochondria did not progress from the tethered to the docked state. Moreover, Fzo1 foci, representing unassembled *trans*-tethering complexes, could not be observed upon mutation of C381. Thus, despite still allowing the formation of *cis* oligomers, mutations in C381 dominantly prevented *trans* oligomerization. Furthermore, Fzo1-C381 mutant variants were not ubiquitylated, leading to abnormally high protein levels. These effects were mostly pronounced in the Fzo1^{C381H} mutant variant, suggesting a sterical hindrance problem. Consistently, C381 is located in helix alpha 4 of the GTPase domain, whose integrity is essential for Fzo1 functionality.^{10,29,30} In sum, mitochondria of cells expressing Fzo1^{C381H} are arrested at an early step in the function of Fzo1, before Fzo1 *trans* association, GTP hydrolysis and ubiquitylation (Figure 6).

Mutations in C805 also compromised mitochondrial OM fusion, albeit differently from C381. In this case, C805 mutations only slightly affect higher oligomerization of Fzo1, meaning that *cis* assembly and *trans* tethering were not majorly affected. Indeed, we could observe the presence of broader protein peaks in C805 mutants, suggesting complex instability. Moreover, Fzo1^{C805S} mutants were still ubiquitylated and extremely unstable, consistent with quality control recognition of abnormally assembled Fzo1. In fact, C805 is located within the HR2 domain. HR2 was shown to be important for the interaction between the N- and C-terminal halves of Fzo1.^{40,47} In particular, C805 is close to hinge 1b, thus probably particularly important for stabilization of the stretched and bent protein conformations.³⁰ In sum, mitochondria of cells expressing Fzo1^{C805S} are arrested at a late step in the function of Fzo1, after Fzo1 *trans* association, GTP hydrolysis and ubiquitylation (Figure 6).

Consistent with the arrest of Fzo1^{C381H} and Fzo1^{C805S} mutants at early and late steps in the OM process, the phenotypes of Fzo1^{C381H} mutations were dominant over those of Fzo1^{C805S}. In conclusion, mutations in Fzo1^{C381} and Fzo1^{C805} arrested the fusion cycle in different steps, playing hierarchical roles in mitochondrial fusion.

Cysteines in yeast vs. mammalian mitofusins

Our study revealed that under constitutive fusion conditions, neither C381 nor C805 was required for cross-linking mediated oligomerization of Fzo1. This suggests that disulfide bond formation does not constitute an intrinsic and conserved requisite for basal fusion of the OM. Thus, elucidation of the specific need for cysteines in positions 381 and 805 of Fzo1, and whether this role is conserved, will require further investigations. In mammals, cysteine residues in MFN2 were identified to be important for mitochondrial hyperfusion, as a response to different metabolic conditions, via modulation of the redox state of the protein and its oligomerization status.³² This effect might depend on particular topologies of mammalian mitofusins, not conserved in yeast, where the C-terminal domain was proposed to be present in the IMS.⁵⁰ These particular MFN1 and MFN2 forms could have a regulatory role in OM fusion, rather than acting as fusogenic molecules directly mediating OM merging.

Ubiquitylation in OM fusion

Ubiquitylation affects proteins either by altering their biochemical properties or by labeling them for degradation via the proteasome.^{51,52} Fzo1 is ubiquitylated in two different ways. On the one hand, short K48-linked ubiquitin chains promote fusion by allowing dissociation of the above-mentioned complex by Cdc48.^{28,29,38,40,42,44,53} On the other hand, under stress, additional destabilizing ubiquitin chains are further assembled, which prime Fzo1 for proteasomal turnover, thereby blocking fusion.^{29,42,44} However, as evidenced by the Fzo1^{C805S} variant, late defects in the OM fusion cascade also trigger proteasomal degradation of Fzo1, impairing OM fusion. Importantly, we could show that proteasome-dependent turnover of Fzo1^{C805S} is causative for the effects on Fzo1 and mitochondrial morphology. Expression of the mutant variant to WT-like levels rescued morphology defects but not protein stability *per se*, demonstrating that in this case mitochondrial fusion was impaired due to insufficient Fzo1 levels.

Proteasomal inhibition as a therapeutic approach in mitofusin-associated diseases

The multitude of neurological and metabolic diseases associated with defects in the mitofusin proteins is not well understood and there is currently no cure available. Thus, a better understanding of the fusion cycle could help determine the disease underlying causes. Tailored point mutants have proven very helpful in dissecting the multistep pathway of mitochondrial OM fusion. The mutation in 381 caused a dominant blockage of the *trans*-complex formation, highlighting the importance of steric hinders in the G-domain dimerization interface. In turn, mutations in the cysteine 805 demonstrated the proteasome as a major quality control regulator of unstable Fzo1 mutants, which prevent OM fusion due to insufficient mitofusin levels. Consistently, the destabilization of the CMT2A homolog mutant variant Fzo1^{T815P} could be rescued by proteasomal inhibition. Proteasomal inhibitors are approved clinical drugs for cancer and neurodegeneration.^{54,55} Thus, our results provide the basis to study the importance of proteasome inhibitors for treating mitofusin-associated diseases linked to low mitofusin levels.

In sum, our analyses shed light on how the interplay between conformational changes and ubiquitylation allows the membrane-embedded version of dynamin-related proteins to promote fusion events. This could help to understand diseases caused by defects in mitofusins and mitochondrial fusion and, in the long run, provide therapeutic directions.

Limitations of the study

This study, while offering basic research on the mechanism of OM fusion, on the proteasomal importance for defects associated with non-functional mitochondrial dynamics, and on how individual amino acids in mitofusins greatly control mitochondrial processes, has two main limitations. These are the amino acid sequence divergence between yeast and metazoans and the need to verify the conservation of our findings in a mammalian model system, especially important to transfer the relevance of our findings for therapeutic application. Future studies are warranted to overcome these limitations.

STAR★METHODS

Detailed methods are provided in the online version of this paper and include the following:

- KEY RESOURCES TABLE
- RESOURCE AVAILABILITY
 - Lead contact

- Materials availability
- Data and code availability
- **EXPERIMENTAL MODEL AND STUDY PARTICIPANT DETAILS**
 - Yeast strains and growth media
 - Plasmids
 - Antibodies
- **METHOD DETAILS**
 - Structural modeling
 - Mitochondrial morphology
 - Mating assay for fusion capacity assessment
 - Isolation of pure mitochondria
 - Electron microscopy
 - Tethering and docking events
 - Identification of Fzo1 foci
 - Isolation of crude mitochondria
 - Fzo1 complex analysis
 - Fzo1 ubiquitylation
 - Co-Immunoprecipitation
 - Total protein cell extraction
 - Protein degradation
 - Cross linking
 - Bradford assay
 - Mass-spectrometry after cross-linking
- **QUANTIFICATION AND STATISTICAL ANALYSIS**
 - Data analysis
 - Statistical analysis

SUPPLEMENTAL INFORMATION

Supplemental information can be found online at <https://doi.org/10.1016/j.isci.2023.107014>.

ACKNOWLEDGMENTS

We would like to thank T Sommer for the Cdc48 and Ubc6 antibodies and ML Mendes for help with the analysis of mass spectrometry after cross-linking. This work was supported by grants from Deutsche Forschungsgemeinschaft (DFG, German Research Foundation) (CRC 1218 TP A03; EXC 2030–390661388; to M.E.-H.), from the Center for Molecular Medicine Cologne (CMMC; CAP14 to M.E.-H. and A02 to M.E.-H. and M.O.), from the Boehringer Ingelheim Foundation (BIS; Exploration grant, to M.E.-H.) and was funded under the Institutional Strategy of the University of Cologne within the German Excellence Initiative (ZUK 81/1, to M.E.-H.).

AUTHOR CONTRIBUTIONS

I.B., V.A., and M.E.-H. designed the study and wrote the manuscript, with input from all authors. I.B. and V.A. performed most experiments and prepared the figures. D.P.-H. performed the mass spectrometry analysis under the supervision of G.D. T.S. performed the Fzo1-Cdc48 co-immunoprecipitations. F.G. performed transmission electron microscopy experiments, under the supervision of A.S. J.R. read the manuscript and provided input on the design of the study. M.E.-H. coordinated the study.

DECLARATION OF INTERESTS

The authors declare no competing interests.

Received: April 27, 2022

Revised: April 23, 2023

Accepted: May 29, 2023

Published: June 7, 2023

REFERENCES

- Dorn, G.W., 2nd (2019). Evolving concepts of mitochondrial dynamics. *Annu. Rev. Physiol.* 81, 1–17. <https://doi.org/10.1146/annurev-physiol-020518-114358>.
- Giacomello, M., Pyakurel, A., Glytsou, C., and Scorrano, L. (2020). The cell biology of mitochondrial membrane dynamics. *Nat. Rev. Mol. Cell Biol.* 21, 204–224. <https://doi.org/10.1038/s41580-020-0210-7>.
- Chan, D.C. (2020). Mitochondrial dynamics and its involvement in disease. *Annu. Rev. Pathol.* 15, 235–259. <https://doi.org/10.1146/annurev-pathmechdis-012419-032711>.
- Yapa, N.M.B., Lisnyak, V., Reljic, B., and Ryan, M.T. (2021). Mitochondrial dynamics in health and disease. *FEBS Lett.* 595, 1184–1204. <https://doi.org/10.1002/1873-3468.14077>.
- Gustafsson, C.M., Falkenberg, M., and Larsson, N.G. (2016). Maintenance and expression of mammalian mitochondrial DNA. *Annu. Rev. Biochem.* 85, 133–160. <https://doi.org/10.1146/annurev-biochem-060815-014402>.
- Mishra, P., and Chan, D.C. (2016). Metabolic regulation of mitochondrial dynamics. *J. Cell Biol.* 212, 379–387. <https://doi.org/10.1083/jcb.201511036>.
- Wai, T., and Langer, T. (2016). Mitochondrial dynamics and metabolic regulation. *Trends Endocrinol. Metabol.* 27, 105–117. <https://doi.org/10.1016/j.tem.2015.12.001>.
- Kraus, F., Roy, K., Pucadyil, T.J., and Ryan, M.T. (2021). Function and regulation of the divisome for mitochondrial fission. *Nature* 590, 57–66. <https://doi.org/10.1038/s41586-021-03214-x>.
- Daumke, O., and Praefcke, G.J.K. (2018). Mechanisms of GTP hydrolysis and conformational transitions in the dynamin superfamily. *Biopolymers* 109, e23079. <https://doi.org/10.1002/bip.23079>.
- Gao, S., and Hu, J. (2021). Mitochondrial fusion: the machineries in and out. *Trends Cell Biol.* 31, 62–74. <https://doi.org/10.1016/j.tcb.2020.09.008>.
- Rapaport, D., Brunner, M., Neupert, W., and Westermann, B. (1998). Fzo1p is a mitochondrial outer membrane protein essential for the biogenesis of functional mitochondria in *Saccharomyces cerevisiae*. *J. Biol. Chem.* 273, 20150–20155.
- Rojo, M., Legros, F., Chateau, D., and Lombès, A. (2002). Membrane topology and mitochondrial targeting of mitofusins, ubiquitous mammalian homologs of the transmembrane GTPase Fzo. *J. Cell Sci.* 115, 1663–1674.
- Mattie, S., Riemer, J., Wideman, J.G., and McBride, H.M. (2018). A new mitofusin topology places the redox-regulated C terminus in the mitochondrial intermembrane space. *J. Cell Biol.* 217, 507–515. <https://doi.org/10.1083/jcb.201611194>.
- Qi, Y., Yan, L., Yu, C., Guo, X., Zhou, X., Hu, X., Huang, X., Rao, Z., Lou, Z., and Hu, J. (2016). Structures of human mitofusin 1 provide insight into mitochondrial tethering. *J. Cell Biol.* 215, 621–629. <https://doi.org/10.1083/jcb.201609019>.
- Cao, Y.L., Meng, S., Chen, Y., Feng, J.X., Gu, D.D., Yu, B., Li, Y.J., Yang, J.Y., Liao, S., Chan, D.C., and Gao, S. (2017). MFN1 structures reveal nucleotide-triggered dimerization critical for mitochondrial fusion. *Nature* 542, 372–376. <https://doi.org/10.1038/nature21077>.
- Yan, L., Qi, Y., Huang, X., Yu, C., Lan, L., Guo, X., Rao, Z., Hu, J., and Lou, Z. (2018). Structural basis for GTP hydrolysis and conformational change of MFN1 in mediating membrane fusion. *Nat Struct Mol Biol.* <https://doi.org/10.1038/s41594-018-0034-8>.
- Li, Y.J., Cao, Y.L., Feng, J.X., Qi, Y., Meng, S., Yang, J.F., Zhong, Y.T., Kang, S., Chen, X., Lan, L., et al. (2019). Structural insights of human mitofusin-2 into mitochondrial fusion and CMT2A onset. *Nat. Commun.* 10, 4914. <https://doi.org/10.1038/s41467-019-12912-0>.
- Low, H.H., and Löwe, J. (2006). A bacterial dynamin-like protein. *Nature* 444, 766–769. <https://doi.org/10.1038/nature05312>.
- Low, H.H., Sachse, C., Amos, L.A., and Löwe, J. (2009). Structure of a bacterial dynamin-like protein lipid tube provides a mechanism for assembly and membrane curving. *Cell* 139, 1342–1352. <https://doi.org/10.1016/j.cell.2009.11.003>.
- Züchner, S., Mersiyanova, I.V., Muglia, M., Bissar-Tadmouri, N., Rochelle, J., Dadali, E.L., Zappia, M., Nelis, E., Patitucci, A., Senderek, J., et al. (2004). Mutations in the mitochondrial GTPase mitofusin 2 cause Charcot-Marie-Tooth neuropathy type 2A. *Nat. Genet.* 36, 449–451. <https://doi.org/10.1038/ng1341>.
- Barbullushi, K., Abati, E., Rizzo, F., Bresolin, N., Comi, G.P., and Corti, S. (2019). Disease modeling and therapeutic strategies in CMT2A: state of the art. *Mol. Neurobiol.* 56, 6460–6471. <https://doi.org/10.1007/s12035-019-1533-2>.
- Hernández-Alvarez, M.I., Sebastián, D., Vives, S., Ivanova, S., Bartocioni, P., Kakimoto, P., Plana, N., Veiga, S.R., Hernández, V., Vasconcelos, N., et al. (2019). Deficient endoplasmic reticulum-mitochondrial phosphatidylserine transfer causes liver disease. *Cell* 177, 881–895.e17. <https://doi.org/10.1016/j.cell.2019.04.010>.
- Chen, L., Liu, B., Qin, Y., Li, A., Gao, M., Liu, H., and Gong, G. (2021). Mitochondrial fusion protein Mfn2 and its role in heart failure. *Front. Mol. Biosci.* 8, 681237. <https://doi.org/10.3389/fmolb.2021.681237>.
- Escobar-Henriques, M., and Anton, F. (2013). Mechanistic perspective of mitochondrial fusion: tubulation vs. fragmentation. *Biochim. Biophys. Acta* 1833, 162–175. <https://doi.org/10.1016/j.bbamer.2012.07.016>.
- Cohen, M.M., and Taresté, D. (2018). Recent insights into the structure and function of Mitofusins in mitochondrial fusion. *F1000Res.* 7, 1983. F1000 Faculty Rev-198312688/f1000research.16629.1.
- De Vecchis, D., Brandner, A., Baaden, M., Cohen, M.M., and Taly, A. (2019). A molecular perspective on mitochondrial membrane fusion: from the key players to oligomerization and tethering of mitofusin. *J. Membr. Biol.* 252, 293–306. <https://doi.org/10.1007/s00232-019-00089-y>.
- Escobar-Henriques, M., and Anton, V. (2020). Mitochondrial surveillance by cdc48/p97: MAD vs. Membrane fusion. *Int. J. Mol. Sci.* 21, 6841. <https://doi.org/10.3390/ijms21186841>.
- Anton, V., Bunttenbroich, I., Schuster, R., Babatz, F., Simões, T., Altin, S., Calabrese, G., Riemer, J., Schauss, A., and Escobar-Henriques, M. (2019). Plasticity in salt bridge allows fusion-competent ubiquitylation of mitofusins and Cdc48 recognition. *Life Sci. Alliance* 2, e201900491. <https://doi.org/10.26508/lsa.201900491>.
- Schuster, R., Anton, V., Simões, T., Altin, S., den Brave, F., Hermanns, T., Hospelthal, M., Komander, D., Dittmar, G., Dohmen, R.J., and Escobar-Henriques, M. (2020). Dual role of a GTPase conformational switch for membrane fusion by mitofusin ubiquitylation. *Life Sci. Alliance* 3, e201900476. <https://doi.org/10.26508/lsa.201900476>.
- De Vecchis, D., Cavellini, L., Baaden, M., Hénin, J., Cohen, M.M., and Taly, A. (2017). A membrane-inserted structural model of the yeast mitofusin Fzo1. *Sci. Rep.* 7, 10217. <https://doi.org/10.1038/s41598-017-10687-2>.
- Thaher, O., Wolf, C., Dey, P.N., Pouya, A., Wüllner, V., Tenzer, S., and Methner, A. (2018). The thiol switch C684 in Mitofusin-2 mediates redox-induced alterations of mitochondrial shape and respiration. *Neurochem. Int.* 117, 167–173. <https://doi.org/10.1016/j.neuint.2017.05.009>.
- Shutt, T., Geoffrion, M., Milne, R., and McBride, H.M. (2012). The intracellular redox state is a core determinant of mitochondrial fusion. *EMBO Rep.* 13, 909–915. <https://doi.org/10.1038/embo.2012.128>.
- Ahmad, S., Khan, H., Shahab, U., Rehman, S., Rafi, Z., Khan, M.Y., Ansari, A., Siddiqui, Z., Ashraf, J.M., Abdullah, S.M., et al. (2017). Protein oxidation: an overview of metabolism of sulphur containing amino acid, cysteine. *Front. Biosci.* 9, 71–87. <https://doi.org/10.2741/s474>.
- Szworst-Lupina, D., Rusinowski, Z., and Zagdańska, B. (2015). Redox modifications of cysteine residues in plant proteins. *Postepy Biochem.* 61, 191–197.
- Kilgore, H.R., and Raines, R.T. (2018). $n \rightarrow \pi^*$ interactions modulate the properties of

- cysteine residues and disulfide bonds in proteins. *J. Am. Chem. Soc.* 140, 17606–17611. <https://doi.org/10.1021/jacs.8b09701>.
36. Kohl, J.B., Mellis, A.T., and Schwarz, G. (2019). Homeostatic impact of sulfite and hydrogen sulfide on cysteine catabolism. *Br. J. Pharmacol.* 176, 554–570. <https://doi.org/10.1111/bph.14464>.
 37. Nunnari, J., Marshall, W.F., Straight, A., Murray, A., Sedat, J.W., and Walter, P. (1997). Mitochondrial transmission during mating in *Saccharomyces cerevisiae* is determined by mitochondrial fusion and fission and the intramitochondrial segregation of mitochondrial DNA. *Mol. Biol. Cell* 8, 1233–1242. <https://doi.org/10.1091/mbc.8.7.1233>.
 38. Anton, F., Fres, J.M., Schauss, A., Pinson, B., Praefcke, G.J.K., Langer, T., and Escobar-Henriques, M. (2011). Ugo1 and Mdm30 act sequentially during Fzo1-mediated mitochondrial outer membrane fusion. *J. Cell Sci.* 124, 1126–1135. <https://doi.org/10.1242/jcs.073080>.
 39. Chappie, J.S., Acharya, S., Leonard, M., Schmid, S.L., and Dyda, F. (2010). G domain dimerization controls dynamin's assembly-stimulated GTPase activity. *Nature* 465, 435–440. <https://doi.org/10.1038/nature09032>.
 40. Cohen, M.M., Amiot, E.A., Day, A.R., Lebouche, G.P., Pryce, E.N., Glickman, M.H., McCaffery, J.M., Shaw, J.M., and Weissman, A.M. (2011). Sequential requirements for the GTPase domain of the mitofusin Fzo1 and the ubiquitin ligase SCFMdm30 in mitochondrial outer membrane fusion. *J. Cell Sci.* 124, 1403–1410. <https://doi.org/10.1242/jcs.079293>.
 41. Brandt, T., Cavellini, L., Kuhlbrandt, W., and Cohen, M.M. (2016). A mitofusin-dependent docking ring complex triggers mitochondrial fusion in vitro. *Elife* 5. <https://doi.org/10.7554/eLife.14618>.
 42. Anton, F., Dittmar, G., Langer, T., and Escobar-Henriques, M. (2013). Two deubiquitylases act on mitofusin and regulate mitochondrial fusion along independent pathways. *Mol. Cell.* 49, 487–498. <https://doi.org/10.1016/j.molcel.2012.12.003>.
 43. Hoppins, S., Horner, J., Song, C., McCaffery, J.M., and Nunnari, J. (2009). Mitochondrial outer and inner membrane fusion requires a modified carrier protein. *J. Cell Biol.* 184, 569–581. <https://doi.org/10.1083/jcb.200809099>.
 44. Simoes, T., Schuster, R., den Brave, F., and Escobar-Henriques, M. (2018). Cdc48 regulates a deubiquitylase cascade critical for mitochondrial fusion. *Elife* 7. <https://doi.org/10.7554/eLife.30015>.
 45. Schindelin, J., Arganda-Carreras, I., Frise, E., Kaynig, V., Longair, M., Pietzsch, T., Preibisch, S., Rueden, C., Saalfeld, S., Schmid, B., et al. (2012). Fiji: an open-source platform for biological-image analysis. *Nat. Methods* 9, 676–682. <https://doi.org/10.1038/nmeth.2019>.
 46. Sitarz, K.S., Yu-Wai-Man, P., Pyle, A., Stewart, J.D., Rautenstrauss, B., Seeman, P., Reilly, M.M., Horvath, R., and Chinnery, P.F. (2012). MFN2 mutations cause compensatory mitochondrial DNA proliferation. *Brain* 135, e219. <https://doi.org/10.1093/brain/aws049>.
 47. Griffin, E.E., and Chan, D.C. (2006). Domain interactions within Fzo1 oligomers are essential for mitochondrial fusion. *J. Biol. Chem.* 281, 16599–16606. <https://doi.org/10.1074/jbc.M601847200>.
 48. Joaquim, M., and Escobar-Henriques, M. (2020). Role of mitofusins and mitophagy in life or death decisions. *Front. Cell Dev. Biol.* 8.
 49. Escobar-Henriques, M., and Joaquim, M. (2019). Mitofusins: disease gatekeepers and hubs in mitochondrial quality control by E3 ligases. *Front. Physiol.* 10, 517. <https://doi.org/10.3389/fphys.2019.00517>.
 50. Mattie, S., Riemer, J., Wideman, J.G., and McBride, H.M. (2017). A new mitofusin topology places the redox-regulated C terminus in the mitochondrial intermembrane space. *J. Cell Biol.* <https://doi.org/10.1083/jcb.201611194>.
 51. Kwon, Y.T., and Ciechanover, A. (2017). The ubiquitin code in the ubiquitin-proteasome system and autophagy. *Trends Biochem. Sci.* 42, 873–886. <https://doi.org/10.1016/j.tibs.2017.09.002>.
 52. Rape, M. (2018). Ubiquitylation at the crossroads of development and disease. *Nat. Rev. Mol. Cell Biol.* 19, 59–70. <https://doi.org/10.1038/nrm.2017.83>.
 53. Escobar-Henriques, M., Westermann, B., and Langer, T. (2006). Regulation of mitochondrial fusion by the F-box protein Mdm30 involves proteasome-independent turnover of Fzo1. *J. Cell Biol.* 173, 645–650. <https://doi.org/10.1083/jcb.200512079>.
 54. Ross, C.A., and Pickart, C.M. (2004). The ubiquitin-proteasome pathway in Parkinson's disease and other neurodegenerative diseases. *Trends Cell Biol.* 14, 703–711. <https://doi.org/10.1016/j.tcb.2004.10.006>.
 55. Zheng, Q., Huang, T., Zhang, L., Zhou, Y., Luo, H., Xu, H., and Wang, X. (2016). Dysregulation of ubiquitin-proteasome system in neurodegenerative diseases. *Front. Aging Neurosci.* 8, 303. <https://doi.org/10.3389/fnagi.2016.00303>.
 56. Brachmann, C.B., Davies, A., Cost, G.J., Caputo, E., Li, J., Hieter, P., and Boeke, J.D. (1998). Designer deletion strains derived from *Saccharomyces cerevisiae* S288C: a useful set of strains and plasmids for PCR-mediated gene disruption and other applications. *Yeast* 14, 115–132. [https://doi.org/10.1002/\(SICI\)1097-0061\(19980130\)14:2<115::AID-YEA204>3.0.CO;115-132](https://doi.org/10.1002/(SICI)1097-0061(19980130)14:2<115::AID-YEA204>3.0.CO;115-132).
 57. Simões, I.C.M., Fontes, A., Pinton, P., Zischka, H., and Wiekowski, M.R. (2018). Mitochondria in non-alcoholic fatty liver disease. *Int. J. Biochem. Cell Biol.* 95, 93–99. <https://doi.org/10.1016/j.biocel.2017.12.019>.
 58. Roy, A., Kucukural, A., and Zhang, Y. (2010). I-TASSER: a unified platform for automated protein structure and function prediction. *Nat. Protoc.* 5, 725–738. <https://doi.org/10.1038/nprot.2010.5>.
 59. Cox, J., and Mann, M. (2008). MaxQuant enables high peptide identification rates, individualized p.p.b.-range mass accuracies and proteome-wide protein quantification. *Nat. Biotechnol.* 26, 1367–1372. <https://doi.org/10.1038/nbt.1511>.
 60. Schrödinger, L., and DeLano, W. (2020). PyMol. <http://www.pymol.org/pymol>.
 61. Sikorski, R.S., and Hieter, P. (1989). A system of shuttle vectors and yeast host strains designed for efficient manipulation of DNA in *Saccharomyces cerevisiae*. *Genetics* 122, 19–27. <https://doi.org/10.1093/genetics/122.1.19>.
 62. Hermann, G.J., Thatcher, J.W., Mills, J.P., Hales, K.G., Fuller, M.T., Nunnari, J., and Shaw, J.M. (1998). Mitochondrial fusion in yeast requires the transmembrane GTPase Fzo1p. *J. Cell Biol.* 143, 359–373.
 63. Simons, R.W., Houman, F., and Kleckner, N. (1987). Improved single and multicopy lac-based cloning vectors for protein and operon fusions. *Gene* 53, 85–96. [https://doi.org/10.1016/0378-1119\(87\)90095-3](https://doi.org/10.1016/0378-1119(87)90095-3).
 64. Westermann, B., and Neupert, W. (2000). Mitochondria-targeted green fluorescent proteins: convenient tools for the study of organelle biogenesis in *Saccharomyces cerevisiae*. *Yeast* 16, 1421–1427. [https://doi.org/10.1002/1097-0061\(200011\)16:15<1421::Aid-yea624>3.0.Co;2-u](https://doi.org/10.1002/1097-0061(200011)16:15<1421::Aid-yea624>3.0.Co;2-u).
 65. Fritz, S., Weinbach, N., and Westermann, B. (2003). Mdm30 is an F-box protein required for maintenance of fusion-competent mitochondria in yeast. *Mol. Biol. Cell* 14, 2303–2313. <https://doi.org/10.1091/mbc.e02-12-0831>.
 66. Mastronarde, D.N. (2003). SerialEM: a program for automated tilt series acquisition on tecnal microscopes using prediction of specimen position. *Microsc. Microanal.* 9, 1182–1183. <https://doi.org/10.1017/s1431927603445911>.
 67. Unger, A.K., Geimer, S., Harner, M., Neupert, W., and Westermann, B. (2017). Analysis of yeast mitochondria by electron microscopy. *Methods Mol. Biol.* 1567, 293–314. https://doi.org/10.1007/978-1-4939-6824-4_18.
 68. Schuster, R., Simões, T., Brave, F.D., and Escobar-Henriques, M. (2018). Separation and visualization of low abundant ubiquitylated forms. *Bio. Protoc.* 8, e3081. <https://doi.org/10.21769/BioProtoc.3081>.
 69. Liu, C., Apodaca, J., Davis, L.E., and Rao, H. (2007). Proteasome inhibition in wild-type yeast *Saccharomyces cerevisiae* cells. *Biotechniques* 42, 158, 160, 162. <https://doi.org/10.2144/000112389>.
 70. Buntenbroich, I., Simões, T., and Escobar-Henriques, M. (2021). Analysis of protein stability by synthesis shutoff. *Bio. Protoc.* 11, e4225. <https://doi.org/10.21769/BioProtoc.4225>.

71. Wessel, D., and Flügge, U.I. (1984). A method for the quantitative recovery of protein in dilute solution in the presence of detergents and lipids. *Anal. Biochem.* 138, 141–143. [https://doi.org/10.1016/0003-2697\(84\)90782-6](https://doi.org/10.1016/0003-2697(84)90782-6).
72. Puchades, M., Westman, A., Blennow, K., and Davidsson, P. (1999). Removal of sodium dodecyl sulfate from protein samples prior to matrix-assisted laser desorption/ionization mass spectrometry. *Rapid Commun. Mass Spectrom.* 13, 344–349. [https://doi.org/10.1002/\(SICI\)1097-0231\(19990315\)13:5<344::AID-RCM489>3.0.CO;2-V](https://doi.org/10.1002/(SICI)1097-0231(19990315)13:5<344::AID-RCM489>3.0.CO;2-V).
73. Rappsilber, J., Mann, M., and Ishihama, Y. (2007). Protocol for micro-purification, enrichment, pre-fractionation and storage of peptides for proteomics using StageTips. *Nat. Protoc.* 2, 1896–1906. <https://doi.org/10.1038/nprot.2007.261>.
74. Chacko, L.A., and Ananthanarayanan, V. (2019). Quantification of mitochondrial dynamics in fission yeast. *Bio. Protoc.* 9, e3450. <https://doi.org/10.21769/BioProtoc.3450>.

STAR★METHODS

KEY RESOURCES TABLE

REAGENT or RESOURCE	SOURCE	IDENTIFIER
Antibodies		
Rat monoclonal anti-HA	Roche	Cat # 11867423001; RRID: AB_390918
Rabbit monoclonal anti-Ubc6	T. Sommer	N/A
Rabbit polyclonal anti-Fzo1	Simoes et al., 2018 ⁴⁴	N/A
Rabbit monoclonal anti-Cdc48	T. Sommer	N/A
Bacterial and virus strains		
DH5 α competent cells	ThermoFisher Scientific	# 18265017
Chemicals, peptides, and recombinant proteins		
Ponceau S	Serva	#33429.02
MG132 InSolution 10mM in DMSO	Calbiochem	#474791
NG310 - Lauryl Maltose Neopentyl Glycol	Anatrace	NG310 5gm
Cycloheximide InSolution 100mg/ml in DMSO	Merck	#C4859
Bortezomib (BTZ)	Merck	#5043140001
NaOH	Merck	#1.06498.5000
β -Mercaptoethanol	Merck	#M6250-100ML
Trichloroacetic acid (TCA)	Roth	#3744.1
SDS	Roth	#CN30.3
Tris	Roth	#5429.5
NaCl	Roth	#3957.2
DTT	MP	#100597
Bismaleimido hexane (BMH)	ThermoFischer	#22330
1,4-Bismaleimidobutane (BMB)	ThermoFisher	#22331
Bismaleimidethan (BMOE)	ThermoFisher	#22323
Color Prestained Protein Standard, Broad Range	NEB	#P7719
Critical commercial assays		
GE Healthcare Amersham™ ECL™ TM Prime	Amersham	#RPN2232
Deposited data		
MFN1-MGD	Cao et al., 2017 ¹⁵	PDB: 5GOE
MFN2-MGD	Li et al., 2019 ¹⁷	PDB: 6JFK
BDLP (GMPPNP)	Low et al., 2009 ¹⁹	PDB: 2W6D
Experimental models: Organisms/strains		
WT (MATa his3 Δ 1 leu2 Δ 0 met15 Δ 0 ura3 Δ 0)	Brachmann et al., 1998 ⁵⁶	BY4741
Δ fzo1 (MATa his3 Δ 1 leu2 Δ 0 met15 Δ 0 ura3 Δ 0 FZO1::kanMX4)	Brachmann et al., 1998 ⁵⁶	RS111
Δ fzo1 (MATalpha his3 Δ 1 leu2 Δ 0 lys2 Δ 0 ura3 Δ 0 FZO1::kanMX4)	Brachmann et al., 1998 ⁵⁶	TS596
Δ dnm1 Δ fzo1 (MATa his3 Δ 1 leu2 Δ 0 met15 Δ 0 ura3 Δ 0 FZO1::kanMX4 DNM1::kanMX4)	Simoes et al., 2018 ⁵⁷	TS1028
ugo1-2 Δ fzo1 (MATalpha leu2-3, 112 trp1-1 can1-100 ura3-1 ade2-1 his3-11, 15 UGO1-2::kanMX6 FZO1::natNT2)	Anton et al., 2019 ²⁸	VA327

(Continued on next page)

Continued

REAGENT or RESOURCE	SOURCE	IDENTIFIER
Δ pd r 5 (MATa his3 Δ 1 leu2 Δ 0 met15 Δ 0 ura3 Δ 0 PDR5::kanMX4)	Brachmann et al., 1998 ⁵⁶	RS519
cdc48-2 Δ fzo1 (MATa his3 Δ 1 leu2 Δ 0 met15 Δ 0 ura3 Δ 0 CDC48-2::kanMX4 FZO1::natNT2)	Simoes et al., 2018 ⁴⁴	RS430
Oligonucleotides		
See Table S1 for all oligonucleotides used in this study.	N/A	N/A
Recombinant DNA		
See Table S2 for all plasmids used in this study.	N/A	N/A
Software and algorithms		
ImageJ	NIH	https://imagej.nih.gov/ij/
Clustal Omega – Multiple Sequence Alignment	EMBL-EBI	https://www.ebi.ac.uk/Tools/msa/clustalo/
iTasser	Roy et al., 2010 ⁵⁸	https://zhanggroup.org/I-TASSER/about.html
EndNote	N/A	N/A
BioRender	N/A	https://biorender.com/
MaxQuant	Cox and Mann, 2008 ⁵⁹	https://www.maxquant.org/
GraphPad	GraphPad Software, San Diego, California USA,	www.graphpad.com
Adobe Illustrator	Adobe Inc., 2019. <i>Adobe Illustrator</i>	https://adobe.com/products/illustrator
Adobe Photoshop	Adobe Inc., 2019. <i>Adobe Photoshop</i>	https://www.adobe.com/products/photoshop.html
PyMOL	Schrödinger and DeLano, 2020 ⁶⁰ s	http://www.pymol.org/pymol

RESOURCE AVAILABILITY

Lead contact

Further information and requests for resources and reagents should be directed to and will be fulfilled by the lead contact, M. Escobar-Henriques (mafalda.escobar@uni-koeln.de).

Materials availability

The raw data of the mass spectrometry analysis is present in [Figure S3](#). All unique materials generated in this study are available upon request.

Data and code availability

- Raw data that support the findings described in the mass spectrometry after cross-linking and quantification of mitochondrial docking events sections can be found in the supplementary materials.
- This paper does not report original code.
- Any additional information required to re-analyze the data reported in this paper is available from the [lead contact](#) upon request.

EXPERIMENTAL MODEL AND STUDY PARTICIPANT DETAILS

Yeast strains and growth media

We conducted experiments with the yeast *Saccharomyces cerevisiae*. Yeast strains are isogenic to the S288c (Euroscarf). They were grown according to standard procedures to the exponential growth phase at 30°C (unless stated otherwise) on yeast-extract peptone (YP) or synthetic complete (SC) media supplemented with 2% (weight/volume) glucose (D), 2% (weight/volume) raffinose or 2% (weight/volume)

galactose. Cycloheximide (CHX) (Sigma-Aldrich) (100 µg/ml for protein shut down from a stock of 10 mg/ml in H₂O), MG132 (Calbiochem) or BTZ (Thermo Fisher Scientific) (both at 50 µM from a stock of 10 mM in DMSO) was added when indicated. Wild-type yeast strains are referred to as "wt" whereas wild-type proteins are referred to as "WT" throughout the manuscript.

Plasmids

The HA-Fzo1 variants newly created in this study were generated by point mutagenesis in plasmid #10,^{42,53} expressed from the centromeric plasmid pRS316⁶¹: #221, #314, #222, #253, #244, #223, #224, #225, #248, #288, #316, #495, #507, #508, #430, #453, #464, #457, #505, #506, #654, #451, #251, #533, #1002.

The 3xMyc-Fzo1 variants newly created in this study and used for analysis of yeast mating were generated by point mutagenesis in plasmid #350,⁶² under the control of the GAL1 promoter and in the backbone pRS415⁶³: C381S (#531), C805S (#532).

The GFP-Fzo1 variants newly created in this study and used for analysis of Fzo1 clustering were generated by point mutagenesis in plasmid #86,²⁸ expressed from the centromeric plasmid pRS316⁶¹: C381H (#869) and C381H;K464R (#876).

Antibodies

The antibodies anti-HA (1:1000 in 5% milk in TBS; #11867423001; Roche), anti-Ubc6 (1:1000 in 5% milk in TBS, gifted by T Sommer), anti-Fzo1 (1:1000 in 5% milk in TBS⁴⁴) and anti-Cdc48 (1:10000 in 5% milk in TBS, gifted by T Sommer) were used in this study.

METHOD DETAILS

Structural modeling

Structural models of Fzo1 based on MFN1-MGD or BDLP were modelled using iTasser.^{28,58} For Fzo1-MGD, amino acids 61-491 followed by a flexible linker (GSGSGSGGS) and amino acids 826-856 were modelled on MFN1-MGD bound to GDP (PDB: 5GOE), GTP (PDB: 5GOF), GDP-BeF₄⁻ (PDB: 5YEW) or GDP-AlF₃⁻ (PDB: 5GOM).^{15,16} For Fzo1 in a membrane context, amino acids 61-856 were modelled on BDLP bound to GDP (PDB: 2J69) or GMPPNP (PDB: 2W6D).^{18,19} Full length MFN1 and MFN2 were modelled on BDLP bound to GMPPNP (PDB: 2W6D).¹⁹ The obtained structure models were processed using PyMOL (Version 2.0 Schrödinger, LLC).

Mitochondrial morphology

Yeast strains were transformed with mitochondrial-targeted GFP expressed from the centromeric plasmid pYX142⁶⁴ or mCherry expressed from pRS413.⁶¹ Strains were grown on YPD or SC media to the exponential phase and analyzed by epifluorescence microscopy (Axioplan 2; Carl Zeiss MicroImaging, Inc.).⁵³ A 63x oil-immersion objective was used; images were acquired with a camera (AxioCam MRm; Carl Zeiss MicroImaging, Inc.) and processed with Axiovision 4.7 (Carl Zeiss MicroImaging, Inc.).

Mating assay for fusion capacity assessment

For the analysis of mitochondrial fusion capacity, yeast mating was performed in exponentially growing cells of opposite mating types (BY4741 and BY4742)^{62,65} expressing 3xMyc-Fzo1 (#350),⁶² 3xMyc-Fzo1C381S (#531) or 3xMyc-Fzo1C805S (#532) (this study), and additionally expressing mitochondrial matrix targeted GFP (mtGFP) or RFP (mtRFP),⁶⁴ all under the control of the repressible GAL1 promoter. In detail, cells were grown at 30°C to exponential growth phase in SC media supplemented with 2% (weight/volume) raffinose. The media was then supplemented with 2% (weight/volume) galactose, to induce expression of Fzo1, mtGFP and mtRFP. Expression was stopped after 1hr by subsequent supplementation with 2% (weight/volume) glucose for 1h, to prevent expression after the subsequent mating step, which would lead to misleading co-localization. The different mating types were subsequently mixed in the indicated combinations and shifted to YPD, to induce mating, for at least 6h before imaging. The imaged cells were categorized as early or late fusion events, i.e. mated cells before or after formation of a bud, respectively. Fusion capacity represents cells showing colocalization of mtGFP and mtRFP and was scored in at least 50 mated cells.²⁸

Isolation of pure mitochondria

1000 OD₆₀₀ of yeast cells were harvested by centrifugation and cell walls were removed by incubation in 50 mM β -mercaptoethanol in 0.1M Tris, pH 9.4, for 20 min at 30°C, 90 rpm, and subsequent incubation in 3 mg/ml lytic enzyme (ICN) in 1.2M sorbitol for 30 min at 30°C, 90 rpm. Spheroplasts were harvested at 1,500g for 5 min at 4°C and washed with 1.2M Sorbitol. Spheroplasts were then resuspended in ice-cold mitochondria isolation buffer (NMIB) (0.6M sorbitol, 5 mM MgCl₂, 50 mM KCl, 100 mM KOAc, and 20 mM Hepes, pH 7.4) and homogenized using a tight dounce on ice 50 times. Unlysed cells and debris were removed from extracts by centrifuging at 3,000g for 5 min at 4°C. Enriched mitochondria were pelleted by centrifuging the supernatant at 10,000g for 10 min at 4°C. Mitochondria-enriched pellets were resuspended in NMIB to a final concentration of 10 mg/ml. Mitochondrial tethering was induced by incubation in stage 1 buffer (20 mM PIPES KOH, pH 6.8, 150 mM KOAc, 5 mM MG(OAc)₂, and 0.6M sorbitol) for 30 min at 4°C. When indicated, mitochondria were treated with 50 μ g/ml trypsin before the tethering reaction as a negative control.²⁸

Electron microscopy

Pure mitochondria extracted as described above were fixed in suspension using 1.5% glutaraldehyde, 3% formaldehyde, and 2.5% sucrose in 0.1M sodium cacodylate buffer over night at 4°C. Mitochondria were pelleted at 13,000g and washed carefully three times with ddH₂O and postfixed with 1% osmium tetroxide for 1 h at 4°C. The pellet was washed four times with ddH₂O and incubated in 0.5% uranyl acetate overnight at 4°C. The pellet was washed three times in ddH₂O and embedded in 2% low-melting agarose, which was cut into small pieces of 1-mm edge length using a razor blade. Agar pieces were dehydrated for 15 min using ascending ethanol concentrations of 50%, 70%, 90%, 2 \times 100%, and 2 \times propylene oxide at 4°C. Pieces were infiltrated with Epon/propylene oxide 1:1 overnight at 4°C and pure Epon for 6 h at RT and embedded into BEEM capsules with conical tip (#69913-01; Science Services) and cured for 48 h at 60°C. Images were acquired using a OneView 4K camera (Gatan) mounted on a Jem-2100Plus (Jeol) transmission electron microscope operating at 200 kV. Large montages of 100 images were acquired using SerialEM.^{28,66,67}

Tethering and docking events

Mitochondrial tethering and docking events we quantified from the images obtained in the transmission electron microscope.²⁸ Mitochondria were quantified as tethered when a distinct membrane contact and changes in membrane curvature were visible. Mitochondria were further quantified as docked when this membrane contact extended over at least one-third of the mitochondrial diameter and a flat contact between two parallel mitochondrial membranes was visible. Mitochondria with a diameter smaller than 100 nm or larger than 1 μ m were excluded from quantification.

Identification of Fzo1 foci

Fzo1-GFP or indicated mutant versions of Fzo1-GFP were co-expressed with a mitochondrial matrix targeted mCherry in $\Delta dnm1\Delta fzo1$ cells and imaged as described for analysis of mitochondrial morphology. In brief, Fzo1-GFP foci were counted as such if they were visible in the GFP marker, but not in the mCherry marker.²⁸

Isolation of crude mitochondria

Exponentially growing yeast cells were harvested and resuspended in TBS with 1 mM PMSF and 750 mg glass beads (0.4–0.6 μ m). Cells were broken upon rigorous vortexing alternated with breaks on ice for a total of 3 min. 600 μ l TBS with 1 mM PMSF was added and the suspension was centrifuged for 3 min at 400g. The supernatant was transferred to a new centrifugation tube. The suspension was centrifuged for 10 min at 16,100g to pellet mitochondria and resuspended in the appropriate buffer for the following experiment.

Fzo1 complex analysis

Fzo1 complex was analyzed by sucrose gradient centrifugation. Crude mitochondria isolated from 55 OD₆₀₀ were dissolved in 50 μ l (for high protein density) or 500 μ l (for low protein density) of solubilization buffer (50 mM Tris-HCl, pH 7.4, 150 mM NaCl, cOmplete protease inhibitor, 1 mM PMSF) with 1% digitonin. After 1 h, the solubilized extracts were centrifuged for 10 min at 16,100g. 9% of the supernatant was kept as input control. Sucrose gradients were prepared in centrifugation tubes (#344059; Beckmann Coulter) as follows: 5% and 25% sucrose solutions were prepared in gradient buffer (50 mM Tris-HCl pH 7.2, 150 mM NaCl, cOmplete protease inhibitor, 0.2% Digitonin). A 5–25% gradient was generated using a gradient mixer (BioComp). The remaining 91% of the supernatant were carefully overlaid on top of the gradient.

The tubes were centrifuged using an ultracentrifuge (SW41Ti rotor, 14–16 h at 4°C, 31,800 rpm). Fractions were collected in 400- μ l steps from the top of the gradient and proteins were precipitated with 14.4% trichloroacetic acid on ice for 20 min. The samples were centrifuged 20 min at 16,100g and 4°C, and the pellet was washed 2 \times with ice-cold acetone. Laemmli buffer was added to the input control and fraction pellets and samples were incubated at 50°C for 10 min and analyzed by SDS–PAGE and immunoblotting, using anti-HA (#11867423001; Roche) antibodies. These analyses have been performed at least five times, leading to consistent results.

Fzo1 ubiquitylation

When indicated, Fzo1 ubiquitylation was analyzed in Fzo1 immunoprecipitated from crude mitochondrial extracts, as described above, obtained from 160 OD₆₀₀ cell pellets of exponentially growing cultures expressing wild-type or mutant variants of HA-Fzo1. After solubilization with NG310 (Lauryl Maltose Neopentyl Glycol; Anatrace), the samples were centrifuged and a portion of the supernatant was kept as input material. To immunoprecipitate HA-tagged Fzo1, the remainder of the supernatant was incubated with HA-coupled beads (Sigma-Aldrich). HA-Fzo1 was eluted in Laemmli buffer and analyzed by SDS–PAGE. Proteins were transferred onto nitrocellulose membranes and subsequently immunoblotted using HA (#11867423001; Roche)-specific antibodies. The analysis of protein ubiquitylation is described in a methods publication.⁶⁸

Co-Immunoprecipitation

Physical interactions between Cdc48 and Fzo1 were analyzed using crude mitochondrial extracts prepared as described above from 160 OD₆₀₀ of exponentially grown yeast cells.⁴⁴ After centrifugation at 16,000g for 10 min, the crude membrane fraction was solubilized using 0.2% NG310 for 1 h rotating at 4°C. HA-Fzo1 was immunoprecipitated using HA-coupled beads (Sigma-Aldrich) rotating overnight at 4°C. Beads were washed three times with 0.2% NG310 in TBS and the precipitated protein was eluted in Laemmli buffer for 20-min shaking at 40°C. 4% of the input and 50% of the eluate fractions were analyzed by SDS–PAGE and immunoblotting, using HA-specific and Cdc48-specific antibodies.

Total protein cell extraction

For analysis of protein steady state levels and ubiquitylation, total proteins from three OD₆₀₀ exponentially growing cells were resuspended in 1 ml of ice-cold water with 260 mM NaOH and 7.5% β -mercaptoethanol and incubated on ice for 15 min. Trichloroacetic acid (TCA) was added to a final concentration of 6.5%, and the suspension was incubated for 10 min on ice. The suspensions were centrifuged at 16,100g for 10 min at 4°C. The supernatant was aspirated and the pellet was dried. The pellet was resuspended in Hydroxy urea buffer (8M Urea, 5% SDS, 200 mM Tris, pH 6.8, 0.01% bromophenol blue, and freshly added 100 mM DTT). Samples were heated to 42°C for 20 min (shaking) before analysis by SDS–PAGE and immunoblotting.

Protein degradation

To monitor protein turnover, cycloheximide (CHX, 100 μ g/ml) was added to exponential cells. Samples of 3 OD₆₀₀ cells were collected at the indicated time points and total proteins were extracted and analyzed as described above. For monitoring proteasome-dependent degradation of cells expressing HA-Fzo1 or HA-Fzo1^{C805S}, cells were treated for 1 h with 50 μ M of the proteasomal inhibitor MG132, before alkaline lysis. In this case, cells were deleted for the multidrug transporter *PDR5*, which prevents cellular detoxification by export of MG132, thus allowing efficient proteasomal inhibition.⁶⁹ The analysis of protein turnover by synthesis shut off is described in a methods publication.⁷⁰

Cross linking

Proteins were cross linked using cysteine specific cross-linking reagents (BMH: 1 μ M–1000 μ M, BMB and BMOE: 100 μ M; DSP: 100 μ M). Crude mitochondrial extracts were prepared by growing 200 OD₆₀₀ of yeast cells in complete media to the exponential growth phase and disrupting cells with glass beads (0.4–0.6 μ m) in TBS. After centrifugation at 16,000g for 10 min the membrane pellet was resuspended in 1x SEM buffer (10 mM MOPS/KOH pH7.2, 250 mM sucrose, 1 mM EDTA) and the protein concentration determined via Bradford assay. Cross-linking reagents were diluted in DMSO and 100 μ g of protein used for each reaction. Crude membranes were treated with the cross-linker, or DMSO as a control, in 50 μ l final volume of 1x SEM buffer for 30 min, RT on a rotating platform. Afterwards, the reaction was stopped by addition of 0.1% β -mercaptoethanol (for BMH; BMB and BMOE) and incubation on ice (15 min). After centrifugation (5 min, 16,100xg, 4°C), the cell pellet was resuspended in 2x SDS sample buffer containing 100 mM DTT.

Bradford assay

The Bradford test is used to determine the total protein amount of a sample. Proteins get linked to Coomassie dye under acidic conditions, resulting in a color range from brown to blue, measuring the presence of basic amino acids within the sample (He, 2011). In the beginning, a dilution series of a reference protein (IgG, BioRad #5000005) is prepared in duplicates in a 96-well plate. Afterwards, unknown samples are diluted 1:25 in water, in duplicates and 200 μ l Bradford reagent (Merck, B2616-500ml) added to each well. After 5 min of incubation, samples are read at 595 nm in a plate reader. Protein concentration is calculated compared to the standard curve.

Mass-spectrometry after cross-linking

Cells lacking *FZO1* expressing either WT Fzo1 or the mutant variants C381S or C805S were grown according to standard procedures in 200ml synthetic media, until an exponential growth phase. 200 OD₆₀₀ were harvested via centrifugation at 4°C and crude mitochondrial extracts were prepared. The protein concentration was determined via Bradford assay and cross-linking was performed on 100 μ g protein by using 100 μ M BMH in a final volume of 50 μ l. After 30min of cross-linking at room temperature, the reaction was stopped as described above (see cross-linking chapter). Crude mitochondria were centrifuged afterwards for 5min at 4°C. The supernatant was removed and the pellet resuspended in lysis buffer (150 mM NaCl, 50 mM Tris pH 7.5, 1% IGPAL-CA-630 (Sigma, #I8896), 5% Glycerol, Protease and phosphatase inhibitors). Acid glass beads (Sigma, 425-600 μ m), on 50 mM Tris-HCl buffer pH 8 were added and, after vortexing, SDS was added to a final amount of 0.2%, being the samples incubated for 10 minutes on ice. Yeast cell cultures were lysed by vortexing with acid glass beads (Sigma, 425-600 μ m). To extract the proteins, the samples were centrifuged at maximum speed in a tabletop centrifuge for 10 minutes. The supernatants were transferred in a new tube. Protein concentration was then measured using the BCA protein kit (Pierce, Thermo Scientific). From each sample, 50 μ g of protein were taken in duplicate. Proteins were reduced with 10 mM DTT for 30 min and alkylated with 55 mM iodoacetamide for 30 min. Wessel-Flügge precipitation was performed as described.^{71,72} The proteome was digested using an automated HTS PAL system (CTC Analytics) (Kanashova et al., 2015). Peptides were extracted, purified, and stored on reversed-phase (C18) StageTips.⁷³ The eluted peptides were lyophilized and resuspended in 0.1% formic acid/3% acetonitrile, then separated in a nano Dionex 3000 Ultimate (Thermo Fisher Scientific) with a Acclaim™ PepMap™ 100 C18 (Thermo Fisher Scientific) at a gradient from 2% to 95% B (100% acetonitrile, 0.1% formic acid) and a flow rate of 300 nl/min in 100 min. The UHPLC was coupled online to an Orbitrap Q Exactive plus mass spectrometer (Thermo Fisher Scientific) for mass spectrometry analysis. The mass spectrometer was set to acquire full-scan MS spectra (300–1700 m/z) at a resolution of 17,500 after accumulation to an automated gain control target value of 1×10^6 and maximum injection time of 20 ms, and was operated in a data-dependent acquisition mode, selecting the 10 most abundant ions for MS/MS analysis, with dynamic exclusion enabled (20 s). Charge state screening was enabled, and unassigned charge states and single charged precursors excluded. Ions were isolated using a quadrupole mass filter with a 1.2 m/z isolation window, with a maximum injection time of 60 ms. HCD fragmentation was performed at a normalized collision energy of 26. The recorded spectra were searched against yeast database from Uniprot (January 2019) using the MaxQuant software package (version 1.6.1.4)⁵⁹ (with fixed modifications set to carbamylation of cysteines and variable modifications set to methionine oxidation, N-terminal acetylation (protein)). Peptide tolerance was 4.5 ppm, and the minimum ratio for LFQ was set to 2. The false discovery rate was set to 1% on protein and peptide level. Statistical analysis of the dataset was performed using R statistical software package (version 3.4.1), Protigy (version 0.8.2), and Perseus software (version 1.6.0.7). For data analysis, proteins that were only identified by site or were potential contaminants were excluded.

QUANTIFICATION AND STATISTICAL ANALYSIS

Data analysis

Quantifications of mitochondrial morphology are depicted as mean (bars), median (line), and individual replicates (circles, squares, triangles and rhombi), from three to four independent experiments with at least 200 cells. Automated quantification of mitochondrial morphology was performed in 30 randomly selected cells per condition, using particle analysis in Fiji / ImageJ.^{45,74} For each cell, the number of counted particles per cell, the average particle size in each cell and the average aspect ratio, i.e. the ratio of the major to the minor axis, is measured and individually represented.

In western blot analyses, protein intensities have been quantified by using a minimum of $n=3$, whereas n indicates the number of biological replicates. Data are displayed in quantifications with standard error of the mean (SEM).

Fzo1 foci formation from at least 100 cells showing a tubular mitochondrial network were counted from three independent experiments. Data are displayed as mean (bars) and individual experiments (circles, squares and triangles).

The ratio indicated in the quantification of mitochondrial docking events is defined by the number of docked mitochondria (D) among all mitochondria in contact (docked plus tethered mitochondria (T)), meaning $(D / (T+D))$, for each of the two independent experiments. Total represents the total number of imaged mitochondria.

Statistical analysis

Statistical analyses are described in the corresponding figure legends, when applicable. Significance tests have been performed by using ANOVA test calculations, displayed as * with $p<0.05$, ** with $p<0.01$, *** with $p<0.001$ and **** with $p<0.0001$ or ns for non significant.